

Electroweak right-handed neutrino portal dark matter

Wan-Zhe Feng*, Ao Li†, Zong-Huan Ye‡, Zi-Hui Zhang§

*Center for Joint Quantum Studies and Department of Physics,
School of Science, Tianjin University, Tianjin 300350, P.R. China*

December 12, 2025

Abstract

We study dark matter coupled to the standard model via electroweak scale right-handed neutrinos in a Type-I seesaw framework. We consider a minimal dark sector containing a fermion χ and a complex scalar ϕ whose only connection to the standard model is through renormalizable Yukawa interactions with right-handed Majorana neutrinos, thus realizing a neutrino portal after seesaw mixing. We discuss three representative realizations of electroweak right-handed neutrinos arising from the Type-I seesaw mechanism, spanning small, large, and ultraweak couplings to the standard model sector, so that the dark particles can either undergo secluded freeze-out or be produced via freeze-in. Instead of merely estimating the order of magnitude of the seesaw couplings, we use the Particle Swarm Optimization algorithm to obtain viable seesaw parameter sets consistent with neutrino data and other constraints, and then compute the coupled evolution of the dark particles and right-handed neutrinos, reproducing the observed dark matter relic abundance in representative benchmark scenarios. For the freeze-in case, we show that internal dark sector interactions can significantly modify the predicted relic density: treating each hidden particle as an independent freeze-in component and simply adding late decays can misestimate the final dark matter abundance by 30%, or even 95%, depending on the type of internal interactions, compared to a full solution of the coupled Boltzmann equations for all dark species, including the dark sector temperature. Electroweak right-handed neutrino portal dark matter thus provides a robust, testable framework that tightly connects neutrino physics, collider searches for heavy neutral leptons, and the cosmological dark matter relic density, offering a well-motivated benchmark for multi-messenger probes at the high energy frontier.

*Email: vicf@tju.edu.cn

†Email: leo_6626@tju.edu.cn

‡Email: y2953083702@tju.edu.cn

§Email: zhangzh_@tju.edu.cn

Contents

1	Introduction	3
2	Type-I seesaw mechanism and generalizations	5
2.1	A consistent Type-I seesaw mechanism revisit	5
2.2	SM neutrino masses from seesaw mixings	6
2.3	Electroweak right-handed neutrino from Type-I seesaw	8
2.3.1	Case-RS: right-handed neutrino from Regular Type-I Seesaw	8
2.3.2	Case-SC: right-handed neutrino from Structure Cancellation	9
2.3.3	Case-SS: right-handed neutrino from Split Seesaw	10
2.3.4	Determine the seesaw parameters	11
3	Right-handed neutrino portal dark matter	12
4	Benchmarks and evolution of the dark particles	14
4.1	Experimental constraints on the right-handed neutrinos	14
4.2	Boltzmann equations	18
4.3	Evolution of the benchmark models	21
4.3.1	Freeze-out evolution, Case-RS, SC	21
4.3.2	Freeze-in evolution, Case-RS, SC, SS	22
5	Conclusion	29
A	Notations and useful formulas	30
B	Seesaw mechanism for one generation, details	32
C	PMNS parameterizations and the Dirac phase	36
D	Non-unitarity constraint	37
E	Scattering processes involving Majorana fermions	38
F	RIS subtraction	40
G	Relevant Feynman diagrams	41
H	Multi-temperature universe and evolution of hidden sector particles	41
I	Seesaw benchmark models	44

1 Introduction

The existence of non-baryonic dark matter (DM) is firmly established by a wide range of astrophysical and cosmological observations, yet its particle nature remains unknown. At the same time, the discovery of neutrino oscillations has demonstrated that neutrinos are massive and mix, providing clear evidence for physics beyond the Standard Model (SM). A natural question is whether the origin of neutrino masses and the nature of dark matter can be linked in a unified framework.

From a theoretical perspective, the Type-I seesaw mechanism is the simplest realization of the effective Weinberg dimension-5 operator for the neutrino mass generation: light neutrino masses are generated by integrating out heavy right-handed Majorana neutrinos, which are singlets of the SM gauge group, without introducing additional $SU(2)_L$ multiplets. In contrast, Type-II and Type-III seesaw mechanisms require an extra scalar $SU(2)_L$ triplet Higgs and a fermionic $SU(2)_L$ triplet, respectively. The chargeless nature of heavy Majorana right-handed neutrinos allows for lepton number violation and provides a natural setting for leptogenesis, while at the same time these singlet fermions can serve as portals to secluded dark sectors.

If the Majorana masses of the right-handed neutrinos lie close to the electroweak scale, rather than at some extremely high energy scale, e.g., GUT scale as commonly studied, it is plausible that the origins of both the electroweak scale and the seesaw scale are interconnected. From an experimental standpoint, this mass range is particularly attractive: electroweak to TeV-scale right-handed neutrinos are potentially accessible at high energy colliders, and the corresponding signatures, such as displaced vertices and lepton number violation [1–7], as well as deviations from unitarity in the lepton mixing matrix [8], can be probed in current and future facilities. Moreover, constraints on TeV-scale right-handed neutrinos are often less stringent than those on very light sterile neutrinos, which are tightly constrained by cosmology [9–12], meson decays [13–15], and precision low-energy experiments [16, 17]. Electroweak scale implementations of the seesaw mechanism are therefore both theoretically motivated and experimentally testable.

In parallel, the persistent absence of signals in direct detection experiments challenges the standard WIMP picture, in which dark matter couples appreciably to quarks. Neutrino portal scenarios offer a compelling alternative: dark matter resides in a hidden sector and communicates with the SM almost exclusively through right-handed neutrinos. In such models, dark matter does not automatically couple to baryons at tree level, and the elastic scattering cross-section off nuclei can naturally lie far below the sensitivity of current and near-future direct detection experiments. At the same time, the same portal fields control both the neutrino mass generation and the dark sector phenomenology, leading to a tightly interconnected structure. Depending on the strength of the right-handed neutrino coupling to the SM and to the dark particles, the hidden sector may be weakly or ultraweakly coupled to the SM [18], leading either to freeze-out evolution [19–24] or to freeze-in production [25–32].

In this work we revisit the Type-I seesaw mechanism with an emphasis on electroweak scale right-handed neutrinos and their role as portals to a dark sector. We consider a minimal dark sector containing a fermion χ and a complex scalar ϕ , stabilized by an appropriate symmetry, and assume that its only renormalizable connection to the SM is provided by Yukawa couplings to right-handed neutrinos. After seesaw mixing, dark sector particles interact with

SM particles through light and heavy neutrinos in the mass eigenstates. Depending on the size of the Yukawa couplings and the seesaw parameters, the dark sector may thermalize with the SM bath and undergo a conventional freeze-out, or it may remain out of equilibrium and be populated via freeze-in. In the latter case, both χ and ϕ can in principle contribute to the present-day DM abundance.

To organize the discussion, we identify three representative realizations of electroweak scale right-handed neutrinos: the regular seesaw (Case-RS), the structure cancellation scenario (Case-SC), and the split seesaw (Case-SS). These cases span small, sizeable, and extremely feeble couplings of the electroweak right-handed neutrinos to the SM, while all reproduce the observed light neutrino masses and mixings. Using the Particle Swarm Optimization (PSO) algorithm, we determine viable seesaw parameter sets for each case and construct benchmark models compatible with neutrino oscillation data and other relevant constraints. In this way, the right-handed neutrino couplings to the SM are determined precisely in each benchmark model, rather than being roughly estimated only at the order-of-magnitude level as in much of the existing literature. We find that the evolution of all dark particles can be completely determined by the seesaw mechanism together with the right-handed neutrino couplings to the dark sector.

We analyze both freeze-out and freeze-in production in Cases RS, SC, and SS. We highlight a common but incorrect approximation in the freeze-in literature, where dark sector internal interactions are ignored and different species are treated as independent freeze-in components. We explicitly show that this approximation can misestimate the final dark matter abundance by about 30% when the hidden sector possesses sufficiently strong three-point internal interactions, and by more than 95% when such interactions are absent, demonstrating that a careful treatment of hidden sector dynamics is essential in right-handed neutrino portal freeze-in models. A key aspect of our analysis is the treatment of the visible sector and the dark sector as a multi-temperature system [33–37]. When hidden sector interactions are strong enough, χ and ϕ can reach internal thermal equilibrium at a hidden temperature T_h distinct from the visible temperature T_v , and the evolution must be described by coupled Boltzmann equations for the comoving number densities and the temperature ratio $\eta \equiv T_v/T_h$. When hidden sector interactions are too weak, the dark sector never equilibrates and the standard freeze-in treatment can apply.

The remainder of this paper is organized as follows. Starting from a general discussion of the Type-I seesaw mechanism, in Section 2 we review the Type-I seesaw mechanism and generalizations at the electroweak scale and outline the three representative cases (RS, SC, SS). In Section 3 we introduce the right-handed neutrino portal dark sector and classify the relevant interactions. Section 4 is devoted to the evolution of dark sector particles via either freeze-out or freeze-in, in concordance with existing neutrino data. We conclude and discuss future directions in Section 5. Useful theoretical details are provided in the Appendices. In particular, in Appendix B we present the most detailed derivation of the Type-I seesaw mechanism for the one-generation case, which is somehow missing from the existing literature.

2 Type-I seesaw mechanism and generalizations

In this section, we provide a brief review of the Type-I seesaw mechanism and generalizations. We concentrate on the simplest Type-I seesaw mechanism and its variations, featuring three right-handed Majorana neutrinos, with at least one residing in the electroweak region. Electroweak scale right-handed neutrinos are intriguing due to their relatively low mass, which increases the likelihood of detection at colliders, and current constraints remain comparatively weak. Electroweak right-handed neutrinos can also act as portals to dark sectors with $\mathcal{O}(100 \text{ GeV})$ dark matter candidates, placing them among the most promising targets for dark matter searches.

We begin with a general discussion of perspective for new physics model building involving Type-I seesaw mechanism. Our notation and conventions are summarized in Appendix A, followed by a detailed one-generation derivation of the Type-I seesaw mixing using two-component spinor formalism in Appendix B. We then discuss three distinct regions of Type-I seesaw parameter space in which electroweak scale right-handed neutrinos have different coupling strengths to the SM.

In this paper, we use the Particle Swarm Optimization (PSO) algorithm to determine viable seesaw parameter sets for each case and construct benchmark models compatible with neutrino oscillation data and other relevant constraints, and thus the right-handed neutrino couplings to the SM are determined precisely in each benchmark model.

2.1 A consistent Type-I seesaw mechanism revisit

The Type-I seesaw Lagrangian is given by

$$\mathcal{L} \supset -y_{ij}^\nu \bar{L}_i \tilde{H} P_R \mathbb{N}_j + h.c. - \frac{M_i}{2} \bar{\mathbb{N}}_i^c \mathbb{N}_i, \quad (1)$$

where \mathbb{N}_i are the Majorana right-handed neutrinos. The corresponding quantum numbers are

Fields	L	H	\mathbb{N}
$B - L$	-1	0	0

Under this assignment, the term $\bar{L}_i \tilde{H} P_R \mathbb{N}_j$ violates $B - L$; hence $B - L$ cannot be imposed as an exact symmetry, either global or local. From this perspective, since the heavy Majorana fermions \mathbb{N} carry no quantum numbers at all, it is natural to consider the possibility that multiple (potentially far more than three) such heavy states may exist at high energies, each with distinct couplings to the LH operator.

An alternative interpretation of the Type-I seesaw Lagrangian involves imposing $B - L$ as a gauge symmetry. In this case, the original Lagrangian takes the form

$$\mathcal{L} \supset -y_{ij}^\nu \bar{L}_i \tilde{H} P_R N_j + h.c. - y_i^N \Phi \bar{N}_i^c N_i, \quad (2)$$

where N_j are Dirac fermions carrying $B - L$ quantum number, and Φ is the $U(1)_{B-L}$ Higgs field responsible for spontaneously breaking the $B - L$ gauge symmetry at a high scale, commonly assumed to be near the GUT scale. In this scenario, the charge assignments under $U(1)_{B-L}$ are summarized as follows:

Fields	L	H	N	Φ
$B - L$	-1	0	-1	$+2$

From this perspective, the Yukawa interaction $\overline{L}_i \tilde{H} P_R N_j$ is $U(1)_{B-L}$ gauge invariant, while the Majorana mass term for N arises from the last term when Φ acquires its vacuum expectation value. After the spontaneous breaking of the $U(1)_{B-L}$ symmetry, N 's become the massive Majorana particles and, as a result, carry no quantum numbers. In this scenario, the theory requires exactly 3 such right-handed neutrinos N_i , each originally carrying a $B - L$ charge -1 , to cancel the $U(1)_{B-L}$ gauge anomaly. It is natural to expect that all three N_i lie around the same mass scale, determined by the vacuum expectation value of the $U(1)_{B-L}$ Higgs field. Given this structure, any additional mixing between LH and other Majorana fermions appears unlikely.

In summary, the right-handed neutrino with a Majorana mass term can be interpreted in two distinct frameworks:

1. **As a truly neutral Majorana fermion** with no conserved charges. In this interpretation, no lepton-number-related symmetry, whether global or gauged, can be imposed, since $\overline{L}_i \tilde{H} P_R N_j$ explicitly violates both lepton number and $B - L$. In general, **more than three** \mathbb{N} fields may couple to LH .
2. **As a $(B - L)$ -charged Dirac fermion** prior to the $B - L$ symmetry breaking. In this case, the $B - L$ gauge symmetry is preserved at very high energies, and the Majorana mass term for N arises only after spontaneous breaking of $U(1)_{B-L}$ symmetry, typically via the vacuum expectation value of a scalar field. **Precisely three** right-handed neutrinos are needed to cancel the $U(1)_{B-L}$ anomaly.

A theoretically inconsistent treatment found in parts of the literature involves introducing massive Majorana right-handed neutrinos with interactions of the form $\overline{L}_i \tilde{H} P_R N_j + h.c.$, which explicitly violate the $B - L$ symmetry, while simultaneously imposing a $U(1)_{B-L}$ gauge symmetry at low energies. This formulation is self-contradictory, as the Yukawa interactions break the very symmetry one attempts to preserve.

A string theory interpretation of the seesaw mechanism is particularly fruitful in the context of D-brane model building. In this framework, right-handed neutrinos can be realized either as chargeless Majorana fermions arising from closed string modes [38], or as bi-fundamental Dirac fermions originating from open strings stretched between different stacks of D-branes [39–44]. In D-brane constructions, the $U(1)$ charges associated with individual D-branes can be consistently canceled through the inclusion of appropriate instantons localized at brane intersections. As a result, it is often possible to construct a variety of gauge-invariant interactions without explicitly breaking the underlying symmetries. Within string theory constructions, the number of right-handed neutrinos is thus not restricted.

2.2 SM neutrino masses from seesaw mixings

With an illustrative detailed derivation for one-generation neutrino seesaw mixing given in Appendix B, the realistic seesaw scenario includes three generations of left-handed neutrinos,

with three right-handed Majorana neutrinos added to complete the model.¹ The most general Lagrangian is written in the flavor eigenbasis as

$$\mathcal{L}_{\text{mass}} = -y_{ij}^\nu \bar{L}_i \tilde{H} P_R \mathbb{N}_j^0 - \frac{M_i}{2} \overline{\mathbb{N}_i^0} \mathbb{N}_i^0 + h.c. = \frac{m_i}{2} \overline{\mathbb{V}_i} \mathbb{V}_i. \quad (3)$$

The masses $m_{1,2,3}$ are the light neutrino masses $\lesssim 10^{-2}$ eV which should match the observed neutrino data as will be detailed in Section 2.3, and $m_{4,5,6}$ the heavy neutrino masses with $m_4 \approx M_1, m_5 \approx M_2, m_6 \approx M_3$.

The seesaw mixing transfers neutrinos from the flavor eigenbasis to the mass eigenbasis. The flavor eigenstates $\mathbb{V}_{i=1-6}^0$ are a combination of 4-component Majorana fermions made by SM neutrinos

$$\mathbb{V}_1^0 = \begin{pmatrix} \nu_e \\ i\sigma_2 \nu_e^* \end{pmatrix}, \quad \mathbb{V}_2^0 = \begin{pmatrix} \nu_\mu \\ i\sigma_2 \nu_\mu^* \end{pmatrix}, \quad \mathbb{V}_3^0 = \begin{pmatrix} \nu_\tau \\ i\sigma_2 \nu_\tau^* \end{pmatrix}, \quad (4)$$

and right-handed Majorana fermions

$$\mathbb{V}_4^0 = \mathbb{N}_1^0 = \begin{pmatrix} -i\sigma_2 N_1^{0*} \\ N_1^0 \end{pmatrix}, \quad \mathbb{V}_5^0 = \mathbb{N}_2^0 = \begin{pmatrix} -i\sigma_2 N_2^{0*} \\ N_2^0 \end{pmatrix}, \quad \mathbb{V}_6^0 = \mathbb{N}_3^0 = \begin{pmatrix} -i\sigma_2 N_3^{0*} \\ N_3^0 \end{pmatrix}, \quad (5)$$

transform to the mass eigenstates $\mathbb{V}_{i=1-6}$ using a unitary matrix U and vice versa:

$$\mathbb{V}_i = U^{-1} \mathbb{V}_i^0, \quad \text{or} \quad \mathbb{V}_i^0 = U \mathbb{V}_i, \quad (6)$$

and the top-left 3×3 block matrix of the matrix U is Pontecorvo–Maki–Nakagawa–Sakata (PMNS) matrix, c.f., Appendix C, which accounts for the observed mixings of neutrinos

$$(\nu_e \ \nu_\mu \ \nu_\tau)^T = U_{\text{PMNS}} (\nu_1 \ \nu_2 \ \nu_3)^T. \quad (7)$$

Thus the neutrinos in the mass eigenbasis are written explicitly in terms of 4-component Majorana spinors

$$\mathbb{V}_1 = \begin{pmatrix} \nu_1 \\ i\sigma_2 \nu_1^* \end{pmatrix}, \quad \mathbb{V}_2 = \begin{pmatrix} \nu_2 \\ i\sigma_2 \nu_2^* \end{pmatrix}, \quad \mathbb{V}_3 = \begin{pmatrix} \nu_3 \\ i\sigma_2 \nu_3^* \end{pmatrix}, \quad (8)$$

are three light neutrinos in nature, although their nature of being Dirac or Majorana hasn't been confirmed, and

$$\mathbb{V}_4 = \mathbb{N}_1 = \begin{pmatrix} N_1 \\ i\sigma_2 N_1^* \end{pmatrix}, \quad \mathbb{V}_5 = \mathbb{N}_2 = \begin{pmatrix} N_2 \\ i\sigma_2 N_2^* \end{pmatrix}, \quad \mathbb{V}_6 = \mathbb{N}_3 = \begin{pmatrix} N_3 \\ i\sigma_2 N_3^* \end{pmatrix}, \quad (9)$$

are the (not-yet-observed) heavy Majorana fermions.

After the seesaw mixing, all charged current interactions are modified:

$$\mathcal{L}_{W^+} = \frac{g_2}{\sqrt{2}} W_\mu^+ \overline{\nu_{iL}} \gamma^\mu \ell_{iL} = \frac{g_2}{\sqrt{2}} W_\mu^+ \overline{V_{\text{SM}i}} P_R \gamma^\mu \ell_{iL} = \frac{g_2}{\sqrt{2}} W_\mu^+ \overline{\mathbb{V}_i^0} P_R \gamma^\mu \ell_{iL}$$

¹The case where two right-handed Majorana neutrinos are added is also discussed in the literature [45–51], leading to the generation of two light neutrinos and one exactly massless neutrino. We will not discuss this case as there is no compelling reason why nature would have only one massless neutrino, although this case has not yet been ruled out by experiments and is thus still possible.

$$= \frac{g_2}{\sqrt{2}} \sum_{j=1}^6 U_{ij} W_\mu^+ \bar{\mathbb{V}}_j \gamma^\mu P_L \ell_{iL}, \quad (10)$$

$$\begin{aligned} \mathcal{L}_{W^-} &= \frac{g_2}{\sqrt{2}} W_\mu^- \bar{\ell}_{iL} \gamma^\mu \nu_{iL} = \frac{g_2}{\sqrt{2}} W_\mu^- \bar{\ell}_{iL} \gamma^\mu P_L V_{\text{SM}i} = \frac{g_2}{\sqrt{2}} W_\mu^- \bar{\ell}_{iL} \gamma^\mu P_L \mathbb{V}_i^0 \\ &= \frac{g_2}{\sqrt{2}} \sum_{j=1}^6 U_{ij} W_\mu^- \bar{\ell}_{iL} \gamma^\mu P_L \mathbb{V}_j, \end{aligned} \quad (11)$$

and the neutral current coupling is also modified as

$$\begin{aligned} \mathcal{L}_Z &= \frac{g_2}{2 \cos \theta_W} Z_\mu \bar{\nu}_{iL} \gamma^\mu \nu_{iL} = \frac{g_2}{2 \cos \theta_W} Z_\mu \bar{V}_{\text{SM}i} \gamma^\mu P_L V_{\text{SM}i} = \frac{g_2}{2 \cos \theta_W} Z_\mu \bar{\mathbb{V}}_i^0 \gamma^\mu P_L \mathbb{V}_i^0 \\ &= \frac{g_2}{2 \cos \theta_W} Z_\mu \left(\sum_{j=1}^6 U_{ij} \bar{\mathbb{V}}_j \right) \gamma^\mu P_L \left(\sum_{k=1}^6 U_{ik} \mathbb{V}_k \right) \\ &= \frac{g_2}{2 \cos \theta_W} \sum_{j=1}^6 \sum_{k=1}^6 U_{ij} U_{ik} Z_\mu \bar{\mathbb{V}}_j \gamma^\mu P_L \mathbb{V}_k. \end{aligned} \quad (12)$$

The Higgs couplings involving neutrinos are written as:

$$\begin{aligned} \mathcal{L}_H &= -\frac{1}{\sqrt{2}} y_{ij}^\nu h (\nu_i^\dagger N_j + N_j^\dagger \nu_i) = -\frac{1}{\sqrt{2}} y_{ij}^\nu h \left(\bar{\mathbb{V}}_i^0 P_R \mathbb{N}_j^0 + \bar{\mathbb{N}}_j^0 P_L \mathbb{V}_i^0 \right) \\ &= -\frac{1}{\sqrt{2}} y_{ij}^\nu h \left(\sum_{\substack{k=1 \\ i=1,2,3}}^6 U_{ik} \bar{\mathbb{V}}_k P_R \sum_{\substack{l=1 \\ j=4,5,6}}^6 U_{jl} \mathbb{V}_l + \sum_{\substack{l=1 \\ j=4,5,6}}^6 U_{jl} \bar{\mathbb{V}}_l P_L \sum_{\substack{k=1 \\ i=1,2,3}}^6 U_{ik} \mathbb{V}_k \right) \\ &= -\frac{1}{\sqrt{2}} y_{ij}^\nu h \left(\sum_{\substack{k=1 \\ i=1,2,3}}^6 \sum_{\substack{l=1 \\ j=4,5,6}}^6 U_{ik} U_{jl} \bar{\mathbb{V}}_k P_R \mathbb{V}_l + \sum_{\substack{k=1 \\ i=1,2,3}}^6 \sum_{\substack{l=1 \\ j=4,5,6}}^6 U_{ik} U_{jl} \bar{\mathbb{V}}_l P_L \mathbb{V}_k \right). \end{aligned} \quad (13)$$

2.3 Electroweak right-handed neutrino from Type-I seesaw

2.3.1 Case-RS: right-handed neutrino from Regular Type-I Seesaw

The relevant Lagrangian for the regular seesaw mass mixing reads

$$\mathcal{L}_{\text{mass}} = -y_{ij}^\nu \bar{L}_i \tilde{H} P_R \mathbb{N}_j^0 + h.c. - \frac{M_i}{2} \bar{\mathbb{N}}_i^0 \mathbb{N}_i^0, \quad (14)$$

Hereafter, boldface symbols denote matrices. In the basis of two component spinors

$$\left(\mathbf{V}_0^T \quad \mathbf{N}^T \right) = \left(\nu_e \quad \nu_\mu \quad \nu_\tau \quad N_1^0 \quad N_2^0 \quad N_3^0 \right) \quad (15)$$

where $\mathbf{V}_0 \equiv (\nu_e \quad \nu_\mu \quad \nu_\tau)^T$ and $\mathbf{N} \equiv (N_1^0 \quad N_2^0 \quad N_3^0)^T$ are 3×1 column matrices consisting of two-component spinors in the original flavor basis (left-handed SM neutrinos and right-handed component of the Majorana neutrinos), the mass terms are expressed as

$$-\mathcal{L}_{\text{mass}} = \frac{1}{2} (\mathbf{V}_0^\dagger \mathbf{M}_D \mathbf{N} + \mathbf{N}^\dagger \mathbf{M}_D^T \mathbf{V}_0 + \mathbf{V}_0^c \mathbf{M}_D \mathbf{N}^c + \mathbf{N}^{c\dagger} \mathbf{M}_D^T \mathbf{V}_0^c) + \frac{1}{2} \mathbf{M}_N (\mathbf{N}^{c\dagger} \mathbf{N} + \mathbf{N}^\dagger \mathbf{N}^c), \quad (16)$$

where the 3×3 mass matrix \mathbf{M}_D is defined as $\mathbf{M}_{Dij} = \frac{1}{\sqrt{2}}y_{ij}v$, and $\mathbf{M}_N = \text{diag}\{M_i\}$. The seesaw mixing matrix is thus written as

$$\begin{pmatrix} 0 & \mathbf{M}_D \\ \mathbf{M}_D^T & \mathbf{M}_N \end{pmatrix}_{6 \times 6}, \quad (17)$$

which is a direct generalization of Eq. (76) for the one-generation neutrino model. For Case-RS, the sub-eV light neutrino masses can be roughly estimated as

$$m_i \sim \frac{y_i^2 v^2}{2M_i} \quad (18)$$

and two cases are most commonly discussed

- The Majorana mass M_i lie near the GUT scale $\sim 10^{14-15}$ GeV, with Yukawa couplings of $\mathcal{O}(1)$.
- The Majorana masses M_i lie at the electroweak–TeV scale, potentially yielding collider-accessible right-handed neutrinos, with Yukawa couplings to the SM of order $10^{-6} - 10^{-7}$. Such small couplings bring the right-handed neutrinos into equilibrium with the SM only when the cosmic temperature drops to below TeV.

We will focus on the electroweak scale right-handed neutrinos in this paper.

2.3.2 Case-SC: right-handed neutrino from Structure Cancellation

This case has exactly the same form of the mass matrix as Case-RS, i.e., Eq. (17), while the 3×3 mixing matrix, relabeled as $\widetilde{\mathbf{M}}_D$, has a specific structure [52, 53]

$$\widetilde{\mathbf{M}}_D \equiv \frac{v}{\sqrt{2}}\mathbf{Y} + \epsilon\mathbf{X} = \frac{v}{\sqrt{2}} \begin{pmatrix} Y_1 & Y_2 & Y_3 \\ \alpha Y_1 & \alpha Y_2 & \alpha Y_3 \\ \beta Y_1 & \beta Y_2 & \beta Y_3 \end{pmatrix} + \epsilon\mathbf{X}, \quad (19)$$

where ϵ is a tiny real parameter, α, β are real numbers, and \mathbf{X} is a 3×3 matrix with entry values within $[-1, 1]$. $Y_{i=1,2,3}$ are the neutrino Yukawa couplings which need to satisfy a further constraint:

$$\sum \frac{Y_i^2}{M_i} = 0. \quad (20)$$

With the above condition, the rank-1 Yukawa matrix \mathbf{Y} renders the 6×6 seesaw mixing matrix rank-3, implying three exactly massless neutrinos, if the $\epsilon\mathbf{X}$ term in Eq. (19) is absent. Turning on $\epsilon\mathbf{X}$ lifts these zero modes and generates tiny masses for the three light neutrinos.

Although fine-tuning is required to obtain sub-eV light neutrino masses, this is the only case in which electroweak scale right-handed neutrinos can have sizable couplings of order $\mathcal{O}(10^{-2})$ to the SM.

2.3.3 Case-SS: right-handed neutrino from Split Seesaw

The minimal seesaw [45–51] contains only two heavy right-handed Majorana neutrinos and can already produce the observed neutrino masses and mixings, leaving the lightest neutrino exactly massless. It is possible, however, to add a third right-handed Majorana (denoted \mathbb{N}_1) with an arbitrary mass, from eV up to above the TeV scale, while coupling only very weakly to the SM through a Yukawa interaction $y_1^\nu \overline{\mathbb{N}}_1 LH$, with y_1^ν much smaller than in the conventional seesaw. Although \mathbb{N}_1 couples only minimally to the SM, it endows the lightest neutrino with a nonzero mass. We refer to this as the **split seesaw** case (Case-SS). The Lagrangian remains that of Eq. (14), but with all y_{i1} (the couplings of \mathbb{N}_1 to LH) taken to be small. For simplicity, we assume that only the lightest \mathbb{N}_1 , the one minimally coupled to the SM, acts as the portal to the dark sector, while \mathbb{N}_2 and \mathbb{N}_3 do not couple to the dark sector.

This case is equivalent to what is often termed the minimal extended seesaw [54–56]: one adds a sterile gauge-singlet Majorana field $\mathbb{S}^T = (-i\sigma_2 S^*, S)$ with mass m_S . The motivation is to obtain a sterile neutrino \mathbb{S} with essentially arbitrary mass (from eV up to above the TeV scale) in addition to the two or three heavy right-handed Majorana neutrinos of the ordinary seesaw, while keeping its couplings to the SM minimal. In the minimal extended seesaw, \mathbb{S} does not couple directly to LH (the Yukawa $\overline{\mathbb{S}} LH$ is set to zero), but it mixes with the seesaw states \mathbb{N}_i through mass terms. Thus, in addition to Eq. (16), the Lagrangian contains

$$\mathcal{L}_{\text{mass}}^{\text{ME}} = -\frac{M_{Si}}{2} \overline{\mathbb{N}}_i \mathbb{S} - \frac{M_{Si}}{2} \overline{\mathbb{S}} \mathbb{N}_i - \frac{m_S}{2} \overline{\mathbb{S}} \mathbb{S}. \quad (21)$$

where the original minimal extended seesaw often takes $m_S = 0$, whereas here we allow $m_S \neq 0$. In the basis of two-component spinors

$$\left(\mathbf{V}_0^T \quad \mathbf{N}^T \quad S \right) = \left(\nu_e \quad \nu_\mu \quad \nu_\tau \quad N_1^0 \quad N_2^0 \quad S \right), \quad (22)$$

the mass terms are expressed as

$$-\mathcal{L}_{\text{mass}}^{\text{ME}} = \frac{1}{2} (S^\dagger \mathbf{M}_S^T \mathbf{N}^c + \mathbf{N}^\dagger \mathbf{M}_S S^c + S^{c\dagger} \mathbf{M}_S^T \mathbf{N} + \mathbf{N}^{c\dagger} \mathbf{M}_S S) + \frac{1}{2} m_S (S^{c\dagger} S + S^\dagger S^c),$$

giving rise to the seesaw mixing matrix

$$\begin{pmatrix} 0 & \mathbf{M}_D & 0 \\ \mathbf{M}_D^T & \mathbf{M}_N & \mathbf{M}_S \\ 0 & \mathbf{M}_S^T & m_S \end{pmatrix}_{6 \times 6}, \quad (23)$$

where $\mathbf{M}_S = (M_{S1} \ M_{S2})^T$ is a 2×1 one column matrix.

In such scenarios, after the diagonalization of the mass matrix of all Majorana fermions, including all \mathbb{N}_i and \mathbb{S} , the case goes back to the Split Seesaw. In the mass eigenbasis, the mostly- \mathbb{S} Majorana fermion couple to the SM only with tiny coupling, proportional to M_{Si}/M_i where M_i are the masses of \mathbb{N}_i .

2.3.4 Determine the seesaw parameters

The seesaw mixing matrix can be block-diagonalized using the Schur complement

$$\begin{aligned} \begin{pmatrix} 0 & \mathbf{M}_D \\ \mathbf{M}_D^T & \mathbf{M}_N \end{pmatrix} &\rightarrow \begin{pmatrix} \mathbf{1}_{3 \times 3} & -\mathbf{M}_D \mathbf{M}_N^{-1} \\ 0 & \mathbf{1}_{3 \times 3} \end{pmatrix} \begin{pmatrix} 0 & \mathbf{M}_D \\ \mathbf{M}_D^T & \mathbf{M}_N \end{pmatrix} \begin{pmatrix} \mathbf{1}_{3 \times 3} & 0 \\ -\mathbf{M}_N^{-1} \mathbf{M}_D^T & \mathbf{1}_{3 \times 3} \end{pmatrix} \\ &= \begin{pmatrix} -\mathbf{M}_D \mathbf{M}_N^{-1} \mathbf{M}_D^T & 0 \\ 0 & \mathbf{M}_N \end{pmatrix}. \end{aligned} \quad (24)$$

for the case that $m_N^{-1} m_D \ll 1$, the Schur complement of the seesaw mixing matrix is approximately unitary

$$\begin{aligned} &\begin{pmatrix} \mathbf{1}_{3 \times 3} & -\mathbf{M}_D \mathbf{M}_N^{-1} \\ 0 & \mathbf{1}_{3 \times 3} \end{pmatrix} \begin{pmatrix} \mathbf{1}_{3 \times 3} & 0 \\ -\mathbf{M}_N^{-1} \mathbf{M}_D^T & \mathbf{1}_{3 \times 3} \end{pmatrix} \\ &= \begin{pmatrix} \mathbf{1}_{3 \times 3} + \mathbf{M}_D \mathbf{M}_N^{-1} \mathbf{M}_N^{-1} \mathbf{M}_D^T & -\mathbf{M}_D \mathbf{M}_N^{-1} \\ -\mathbf{M}_N^{-1} \mathbf{M}_D^T & \mathbf{1}_{3 \times 3} \end{pmatrix} \approx \mathbf{1}_{6 \times 6} \end{aligned} \quad (25)$$

The top-left 3×3 $\mathbf{M}_D \mathbf{M}_N^{-1} \mathbf{M}_D^T$ will be further diagonalized by

$$\begin{aligned} \begin{pmatrix} -\mathbf{M}_D \mathbf{M}_N^{-1} \mathbf{M}_D^T & 0 \\ 0 & \mathbf{M}_N \end{pmatrix} &\rightarrow \begin{pmatrix} U^T & 0 \\ 0 & \mathbf{1}_{3 \times 3} \end{pmatrix} \begin{pmatrix} -\mathbf{M}_D \mathbf{M}_N^{-1} \mathbf{M}_D^T & 0 \\ 0 & \mathbf{M}_N \end{pmatrix} \begin{pmatrix} U & 0 \\ 0 & \mathbf{1}_{3 \times 3} \end{pmatrix} \\ &= \begin{pmatrix} \mathbf{M}_\nu & 0 \\ 0 & \mathbf{M}_N \end{pmatrix}_{6 \times 6} \end{aligned} \quad (26)$$

In this way, one obtains semi-analytic expressions for the light-neutrino mass eigenvalues and can thereby determine the allowed ranges of all input parameters.

- For Case-RS, there are in total 12 input parameters:

$$\left(y_{ij} \ M_i \right) \quad (27)$$

with the diagonal Yukawa $y_{ii} \in [10^{-7}, 10^{-5}]$, off-diagonal Yukawa $y_{ij} \in [0, 4 \times 10^{-6}]$, and the 3 Majorana masses $M_i \in [100, 300]$.

- For Case-SC, there are in total 17 input parameters:

$$\left(Y_{i=1,2} \ \alpha \ \beta \ \mathbf{X}_{ij} \ \epsilon \ M_1 \ M_2 \ M_3 \right) \quad (28)$$

where the third Yukawa coupling is determined by the condition Eq. (20). The Yukawa coupling $Y_{i=1,2} \in [0.01, 1]$, $\alpha, \beta \in [0.1, 25]$, $\mathbf{X}_{ij} \in [-1, 1]$, $\epsilon \in [10^{-12}, 10^{-8}]$, $M_1, M_2, M_3 \in [100, 300]$.

- For Case-SS, there are also in total 12 input parameters similar to Case-RS:

$$\left(y_{ij} \ M_i \right) \quad (29)$$

with the mass of \mathbb{N}_1 around the electroweak scale, and \mathbb{N}_1 is minimally coupled to the SM with $y_{i1} \in [10^{-10}, 10^{-8}]$. In Case-SS, $\mathbb{N}_2, \mathbb{N}_3$ are assumed not to couple to the

dark sector, so their parameters may span a wide range. Two sets of typical values are: (1) $\mathbb{N}_2, \mathbb{N}_3$ are also around the electroweak scale, with Majorana masses set in the region $M_2, M_3 \in [100, 10^4]$, and the diagonal Yukawa $y_{22}, y_{33} \in [10^{-7}, 10^{-5}]$, off-diagonal Yukawa $y_{i2}, y_{i3} \in [0, 4 \times 10^{-6}]$; or (2) $\mathbb{N}_2, \mathbb{N}_3$ are at the GUT scale, with Majorana masses within $M_2, M_3 \in [10^{14}, 10^{15}]$, and the diagonal Yukawa $y_{i2}, y_{i3} \in [0.01, 1]$. In both cases, $\mathbb{N}_2, \mathbb{N}_3$ do not play a role in the dark sector evolution.

With the given parameters for all above cases, the diagonalization of the seesaw mixing matrix gives rise to the 6×6 rotation matrix U . The upper-left 3×3 block of the rotation matrix U should fit the PMNS matrix determined from neutrino oscillation data:

$$|U_{\text{PMNS}}^{\text{ex}}| = \begin{pmatrix} 0.803 \sim 0.845 & 0.514 \sim 0.578 & 0.142 \sim 0.155 \\ 0.233 \sim 0.505 & 0.460 \sim 0.693 & 0.630 \sim 0.799 \\ 0.262 \sim 0.525 & 0.473 \sim 0.702 & 0.610 \sim 0.762 \end{pmatrix}. \quad (30)$$

The masses of the three light neutrinos should also satisfy: (1) the upper bound of neutrino mass sum, i.e.,

$$\sum_i m_{\nu i} \lesssim 0.12 \text{ eV} \quad (31)$$

(2) the experimental fitting values of the mass-square differences

$$\Delta m_{12}^2 = m_{\nu 2}^2 - m_{\nu 1}^2 = 7.54 \times 10^{-5} \text{ eV}^2, \quad (32)$$

$$\Delta m_{13}^2 = m_{\nu 3}^2 - m_{\nu 1}^2 = 2.47 \times 10^{-3} \text{ eV}^2. \quad (33)$$

We apply the Particle Swarm Optimization (PSO) algorithm to find the values of all the input parameters. The optimization is done by requiring the calculated values from seesaw mixing matrix matching all above mentioned experiment values. To this end, we define 4 fitting functions, which capture the deviation of the calculated $|U_{\text{PMNS}}|$, neutrino mass sum, two mass-square differences to the respective experimental values. We also define a 5th fitting function for Case-SC, ensuring that the non-unitarity constraint is satisfied, which sets limits on the size of the mixing between the SM neutrinos and right-handed neutrinos, as briefly summarized in Appendix D. Such requirement is needed only for considerable large mixings between the SM neutrinos and the right-handed Majorana neutrinos, which is present only for Case-SC among the three cases we consider. The observed Dirac phase can also be incorporated in the search for the seesaw parameters, as explained in Appendix C. All our seesaw benchmark models are summarized in Appendix I.

3 Right-handed neutrino portal dark matter

The right-handed neutrino portal refers to scenarios in which right-handed Majorana neutrinos act as portal mediators to the dark sector. The dark sector consists of a dark fermion χ and a dark complex scalar ϕ , there can be either a dark $U(1)$ symmetry or a dark \mathbb{Z}_2 symmetry protecting the stability of the two particles. If there is a dark $U(1)$ gauge symmetry, in this work we assume the dark $U(1)$ symmetry is already broken at some high scale, and the $U(1)$ gauge boson is very massive and thus not contributing to the dark sector evolution.

The general right-handed neutrino portal Lagrangian is written as

$$\mathcal{L}_{\text{RHNP}} = y_i^x \overline{\mathbb{N}}_i^0 \chi \phi + y_i^{x*} \bar{\chi} \phi^\dagger \mathbb{N}_i^0, \quad (34)$$

where the Yukawa coupling y_i^x can be real or complex, \mathbb{N}_i^0 are the right-handed Majorana fermion in the original flavor basis of the Type-I seesaw interactions. The three Majorana fermions mixed with the three SM neutrinos and after the seesaw mixing, it becomes a linear combination of all six flavor neutrinos in the mass eigenbasis, c.f., Eq. (6). Thus after the seesaw mixing, the right-handed portal interactions are modified to be (the *h.c.* terms are shown explicitly)

$$\begin{aligned} \mathcal{L}_{\text{RHNP}} &= y_i^x \sum_{j=1}^6 U_{ij} \overline{\mathbb{V}}_j \chi \phi + y_i^{x*} \bar{\chi} \phi^\dagger \sum_{j=1}^6 U_{ij} \mathbb{V}_j \\ &= \sum_{j=1}^6 y_i^x U_{ij} \overline{\mathbb{V}}_j \chi \phi + \sum_{j=1}^6 y_i^{x*} U_{ij} \bar{\chi} \phi^\dagger \mathbb{V}_j \\ &\equiv \sum_{i=1}^6 \left[y_i^{x'} \overline{\mathbb{V}}_i \chi \phi + y_i^{x'*} \bar{\chi} \phi^\dagger \mathbb{V}_i \right], \end{aligned} \quad (35)$$

where $y_i^{x'}$ are the hidden sector coupling constants after the seesaw mixing.

As discussed in Section 2.3, the right-handed Majorana fermion can be regarded as either pure neutral Majorana fermion, or originally $B-L$ charged Dirac fermion N_i and becoming a Majorana after a $B-L$ symmetry breaking. In the latter viewpoint, the dark sector particles χ or ϕ may also carry $B-L$ quantum number to balanced the $B-L$ charge originally carried by N_i . Although at low energies the interactions in Eq. (35) already violate $B-L$, any probe of right-handed neutrino portal dark matter is therefore blind to the underlying $B-L$ symmetry (if existed).

In this work we focus on scenarios where the evolutions of both χ and ϕ are determined purely by the right-handed neutrino portal interactions.²

The existence of the interaction terms $\sim \bar{\chi} \phi^\dagger \mathbb{V}_i$ (the discussion for *h.c.* terms are similar), where $\mathbb{V}_{1,2,3}$ are the mass eigenstates of light neutrinos, allows for a decay of either $\chi \rightarrow \bar{\phi} + \mathbb{V}_i$ or $\bar{\phi} \rightarrow \chi + \mathbb{V}_i$ depending the mass hierarchy of χ, ϕ . In this work we always assume $m_\chi < m_\phi$ and thus χ is dark matter. ϕ fully decays before BBN in the freeze-out scenario. In the freeze-in scenario, the couplings between dark sector particles and SM fields are naturally suppressed. It is therefore possible that the dark coupling y_i^x is extremely small, in which case the decays $\bar{\phi} \rightarrow \chi + \mathbb{V}_i$ have lifetimes exceeding the age of the Universe, and both χ and ϕ can serve as dark matter candidates.

The electroweak right-handed neutrino couplings to the SM particles can be determined from the three different types of seesaw mixings, as discussed in the Section 2:

1. For Case-RS, the Yukawa couplings of electroweak right-handed neutrinos to LH is of the order $10^{-7} - 10^{-8}$. Consequently the hidden sector equilibrates with the SM only at late times ($\lesssim \mathcal{O}(\text{TeV})$), but before the dark matter freeze-out.

²Especially in freeze-in scenarios, the masses of the dark $U(1)$ gauge boson and of the $U(1)_{B-L}$ gauge boson (if present) should be larger than the reheating temperature. Otherwise, these $U(1)$ gauge bosons can be copiously produced, bringing all dark sector particles into equilibrium with the SM and thereby violating the freeze-in assumption.

2. For Case-SC, the large Yukawa couplings keep the hidden sector in thermal equilibrium with the bath at early times, after which dark matter undergoes freeze-out.
3. For Case-SS, we assume that only the lightest \mathbb{N}_1 , which couples minimally to the SM, acts as the portal to the dark sector. As a result, the dark sector particles are produced solely via freeze-in.

With the assistance of right-handed neutrinos as a portal connecting hidden and visible sectors, the abundance of dark particles can be efficiently depleted through freeze-out, or generated through freeze-in. All relevant interactions are summarized as follows ($i, j = 1-3$):

1. Particles $\chi, \bar{\chi}, \phi, \bar{\phi}$ annihilate/decay into SM particles, mediated by portal particles \mathbb{N}_i : $\chi\bar{\chi} \rightarrow \mathbb{V}_i\mathbb{V}_j, \phi\bar{\phi} \rightarrow \mathbb{V}_i\mathbb{V}_j, \chi\phi(\bar{\chi}\bar{\phi}) \rightarrow h\mathbb{V}_i, Z\mathbb{V}_i, W^\pm\ell_i^\mp$, and three-point processes $\phi \leftrightarrow \bar{\chi}\mathbb{V}_i$ ($\bar{\phi} \leftrightarrow \chi\mathbb{V}_i$) if $m_\phi > (m_\chi + m_i)$.
2. Particles $\chi, \bar{\chi}, \phi, \bar{\phi}$ transform into portal particles \mathbb{N}_i , followed by \mathbb{N}_i decaying into SM particles: $\chi\bar{\chi} \leftrightarrow \mathbb{V}_i\mathbb{N}_j, \mathbb{N}_i\mathbb{N}_j, \phi\bar{\phi} \leftrightarrow \mathbb{V}_i\mathbb{N}_j, \mathbb{N}_i\mathbb{N}_j, \chi\phi(\bar{\chi}\bar{\phi}) \leftrightarrow h\mathbb{N}_i, Z\mathbb{N}_i$, and three-point channels $\chi\phi(\bar{\chi}\bar{\phi}) \leftrightarrow \mathbb{N}_i$ if $M_i > (m_\chi + m_\phi)$, $\phi \leftrightarrow \bar{\chi}\mathbb{N}_i$ ($\bar{\phi} \leftrightarrow \chi\mathbb{N}_i$) if $m_\phi > (m_\chi + M_i)$.
3. Right-handed neutrinos decay channels: $\mathbb{N}_i \leftrightarrow h\mathbb{V}_j, Z\mathbb{V}_j, W^\pm\ell_i^\mp$, and $\mathbb{N}_i \leftrightarrow \chi\phi(\bar{\chi}\bar{\phi})$ if $M_i > (m_\chi + m_\phi)$.
4. Interactions within the hidden sector: $\chi\chi \leftrightarrow \bar{\phi}\bar{\phi}$ ($\bar{\chi}\bar{\chi} \leftrightarrow \phi\phi$), $\chi\bar{\chi} \leftrightarrow \phi\bar{\phi}$.

The couplings related to the right-handed neutrino portal are summarized as follows:

$$W_\mu^+ \bar{\nu}_{iL} \gamma^\mu \ell_{iL} : \quad \frac{g_2}{\sqrt{2}} \sum_{j=1}^6 U_{ij} W_\mu^+ \bar{\mathbb{V}}_j \gamma^\mu P_L \ell_{iL}, \quad (36)$$

$$W_\mu^- \ell_{iL} \gamma^\mu \nu_{iL} : \quad \frac{g_2}{\sqrt{2}} \sum_{j=1}^6 U_{ij} W_\mu^- \ell_{iL} \gamma^\mu P_L \mathbb{V}_j, \quad (37)$$

$$Z_\mu \bar{\nu}_{iL} \gamma^\mu \nu_{iL} : \quad \frac{g_2}{2 \cos \theta_W} \sum_{j=1}^6 \sum_{k=1}^6 U_{ij} U_{ik} Z_\mu \bar{\mathbb{V}}_j \gamma^\mu P_L \mathbb{V}_k, \quad (38)$$

$$\bar{L}_i \tilde{H} P_R \mathbb{N}_j^0 + h.c. : \quad - \frac{y_{ij}}{\sqrt{2}} h \left(\sum_{k=1,2,3}^6 \sum_{l=1,2,3}^6 U_{ik} U_{jl} \bar{\mathbb{V}}_k P_R \mathbb{V}_l + \sum_{k=1,2,3}^6 \sum_{l=1,2,3}^6 U_{ik} U_{jl} \bar{\mathbb{V}}_l P_L \mathbb{V}_k \right), \quad (39)$$

$$\chi\phi\bar{\mathbb{N}}_i^0 + h.c.. : \quad \sum_{j=1}^6 y_i^x U_{ij} \bar{\mathbb{V}}_j \chi\phi + \sum_{j=1}^6 y_i^{x*} U_{ij} \bar{\chi}\phi^* \mathbb{V}_j. \quad (40)$$

4 Benchmarks and evolution of the dark particles

4.1 Experimental constraints on the right-handed neutrinos

The CMS and ATLAS Collaborations at the LHC have analyzed proton-proton collision data from Drell-Yan and vector boson fusion (VBF) processes [57], placing a range of constraints

on heavy Majorana neutrinos in the Type-I seesaw model for masses ranging from several hundred GeV up to the TeV scale [1–7]. Through their mixing with light neutrinos, the heavy neutrinos \mathbb{N} participate in weak interactions and may appear either as final-state particles or as internal propagators in Drell-Yan and VBF processes. These studies search for signatures of heavy right-handed neutrinos by analyzing the resulting final states. All these studies consider only the mixing between the lightest heavy Majorana neutrino and a single SM neutrino flavor. In addition, the L3 Collaboration has analyzed data from electron-positron collisions at LEP, placing bounds on heavy right-handed neutrinos with masses around 100 GeV [58]. Electroweak precision observables also provide complementary constraints on new leptons that mix with SM leptons [59]. The combined experimental bounds including the electroweak precision test constraints are summarized in Figs. 1, 2 and 3.

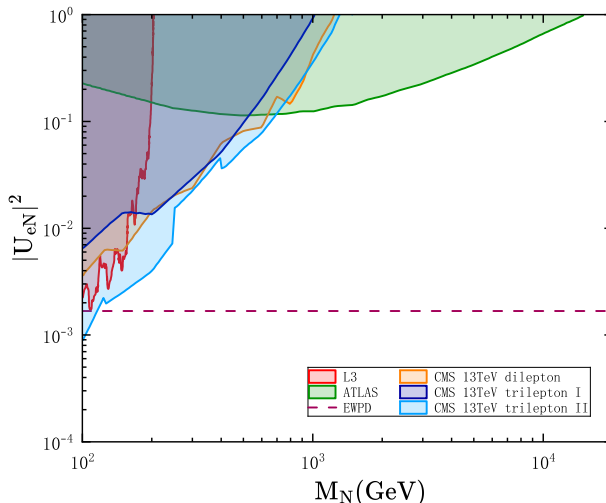


Figure 1: Exclusion limits at the 95% confidence level on the active-sterile mixing parameter $|U_{e\mathbb{N}}|^2$ are presented. The upper bounds are derived from various sources, including L3’s search via $e^+e^- \rightarrow \mathbb{N}\nu$ [58], ATLAS same-sign WW scattering [5], and several CMS analyses at $\sqrt{s} = 13$ TeV: same-sign dilepton [3], trilepton [2,6], as well as global electroweak precision data (EWP) constraints [59].

ATLAS The ATLAS Collaboration has searched for events featuring two muons and hadronic jets in proton-proton collisions at $\sqrt{s} = 13$ TeV, using data collected during 2015–2018 with an integrated luminosity of 140 fb^{-1} . Constraints were placed on the mixing parameter $|U_{\mu\mathbb{N}}|^2$ for a heavy Majorana neutrino \mathbb{N} with masses ranging from 50 GeV to 20 TeV. The analysis targets same-sign $\mu^+\mu^+$ production via vector boson fusion in W^+W^+ scattering, with \mathbb{N} appearing as an intermediate state. The signal region requires events containing same-sign muon pairs along with at least two hadronic jets that are well separated in rapidity. Using the same dataset, ATLAS has also analyzed final states with μe and ee leptons [7], placing constraints on $|U_{e\mathbb{N}}|^2$ and the product $|U_{e\mathbb{N}}U_{\mu\mathbb{N}}^*|$.

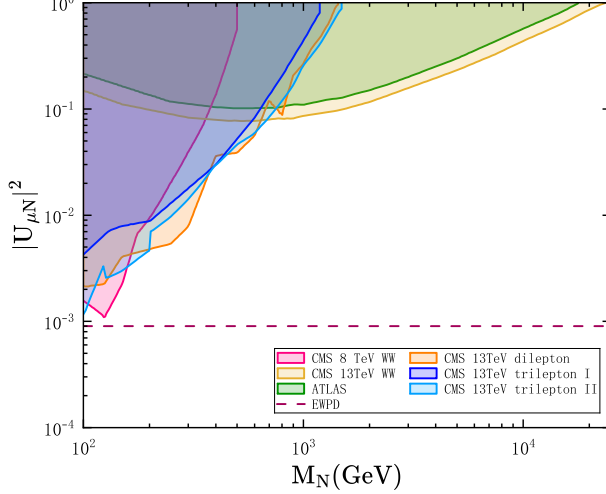


Figure 2: Exclusion limits at the 95% confidence level on the active sterile mixing parameter $|U_{\mu N}|^2$ are presented. The upper bounds are obtained from several sources, including ATLAS same-sign WW scattering [7], CMS same-sign dilepton at $\sqrt{s} = 13$ TeV [3], CMS trilepton analysis [2,6], CMS same-sign WW scattering [4], CMS same-sign dilepton at $\sqrt{s} = 8$ TeV [1], and electroweak precision data (EWP) [59].

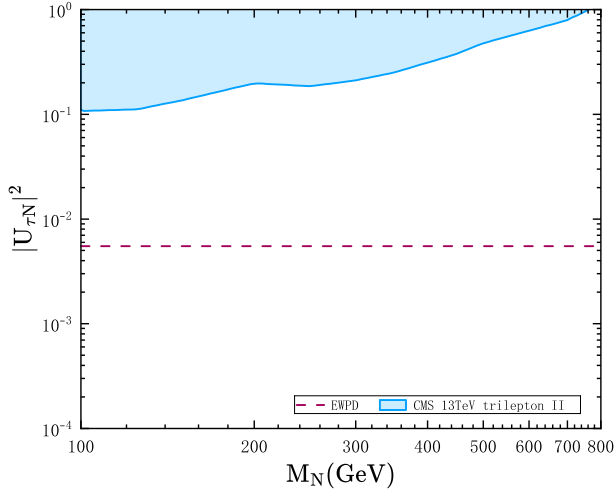


Figure 3: Exclusion limits at the 95% confidence level on the active sterile mixing parameter $|U_{\tau N}|^2$ are presented. The upper bounds are derived from the CMS trilepton analysis at $\sqrt{s} = 13$ TeV [6] and from electroweak precision data (EWP) [60].

CMS The CMS Collaboration has searched for signatures of same-sign dileptons accompanied by jets in proton-proton collisions at $\sqrt{s} = 13$ TeV, using the 2016 dataset with an integrated luminosity of 35.9 fb^{-1} . Constraints were placed on the mixing parameters $|U_{eN}|^2$, $|U_{\mu N}|^2$, and $|U_{eN}U_{\mu N}^*|^2/(|U_{eN}|^2 + |U_{\mu N}|^2)$, for heavy neutrino masses in the range of 20 to 1600 GeV. The signal region was defined by requiring two same-sign leptons in the final state, which significantly suppresses SM backgrounds compared to opposite-sign dilepton channels. In addition, CMS has also searched for same-sign dimuon plus dijet signatures in

proton-proton collisions at $\sqrt{s} = 8$ TeV with an integrated luminosity of 19.7 fb^{-1} [1]. This analysis placed constraints on $|U_{\mu\mathbb{N}}|^2$ for heavy neutrino masses between 40 and 500 GeV.

The W bosons produced in the Drell-Yan and VBF processes can also decay into a charged lepton and a neutrino [2]. The CMS Collaboration has searched for events with three charged leptons in the final state using proton-proton collision data at $\sqrt{s} = 13$ TeV, collected in 2016 with an integrated luminosity of 35.9 fb^{-1} . Constraints were placed on the mixing parameters $|U_{e\mathbb{N}}|^2$ and $|U_{\mu\mathbb{N}}|^2$ for heavy neutrino masses in the range of 1 to 1200 GeV. The analysis targets final states with three charged leptons in any combination of electrons and muons, excluding events in which all three leptons have the same electric charge.

Ref. [6] presents an updated analysis based on a larger dataset collected from 2016 to 2018 at $\sqrt{s} = 13$ TeV with an integrated luminosity of 138 fb^{-1} , and incorporates improved analysis techniques. This study provides more precise constraints on the mixing parameters $|U_{e\mathbb{N}}|^2$, $|U_{\mu\mathbb{N}}|^2$, and $|U_{\tau\mathbb{N}}|^2$ for heavy neutrino masses ranging from 10 GeV to 1500 GeV. The inclusion of τ -flavor mixing is enabled by advancements in τ lepton reconstruction and identification. In addition, the analysis considers both scenarios in which \mathbb{N} is a Majorana or a Dirac fermion.

Using the same underlying mechanism as the ATLAS same-sign W^+W^+ scattering analysis, CMS has conducted a search for the corresponding signal in proton-proton collisions at $\sqrt{s} = 13$ TeV, based on the full Run 2 dataset with an integrated luminosity of 138 fb^{-1} . This analysis places constraints on $|U_{\mu\mathbb{N}}|^2$ for heavy neutrino masses in the range of 50 GeV to 25 TeV [4].

L3 The constraints reported by the L3 Collaboration are based on the following assumptions [58]: each generation of Standard Model neutrinos mixes exclusively with a corresponding heavy isosinglet neutrino. The analysis neglects mixing among the light neutrinos, as well as any mixing between the heavy neutrinos or with additional isodoublet states.

In the electron-positron annihilation process $e^+e^- \rightarrow \mathbb{N}\nu$, the total cross section is dominated by the t -channel exchange of a W boson. Due to LEP's limited sensitivity to the production of \mathbb{N}_μ and \mathbb{N}_τ via this channel, the analysis focuses exclusively on the production of \mathbb{N}_e in association with a ν_e . The heavy neutrino \mathbb{N} subsequently decays via $\mathbb{N} \rightarrow W\ell$ or $\mathbb{N} \rightarrow Z\nu$, with the $W\ell$ channel being dominant, for \mathbb{N} masses near W and Z masses where phase space suppression reduces the branching ratio of the $Z\nu$ channel. The primary signal process is therefore $e^+e^- \rightarrow \mathbb{N}_e\nu_e \rightarrow \nu_e e W \rightarrow \nu_e e q'\bar{q}$, resulting in a final state characterized by a single isolated electron and hadronic jets. Based on this signature, the L3 Collaboration performed a search using e^+e^- collision data collected at LEP with $\sqrt{s} \approx 200$ GeV, and placed constraints on the mixing parameter $|U_{e\mathbb{N}}|^2$ for heavy neutrino masses in the range of 80 – 205 GeV.

Future collider searches Future collider experiments, such as the LHeC and ILC [61,62], present promising opportunities to probe heavy Majorana neutrinos through a variety of production channels. These include electron-positron annihilation processes such as $e^-e^+ \rightarrow N_1\bar{\nu}$, electron-proton scattering processes $eq \rightarrow N_1\bar{q}'$, and electron-photon interactions $e^-\gamma \rightarrow NW^-$. Notably, utilizing photons generated via proton bremsstrahlung leads to cleaner experimental signatures and significantly reduced Standard Model backgrounds compared to

electron bremsstrahlung [62]. These future facilities have the potential to significantly constrain the parameter space of heavy neutrinos with masses at the TeV scale. In addition, the proposed μ TRISTAN collider offers a unique platform to explore heavy neutrinos via electron-muon collisions, specifically through the process $e^- \mu^+ \rightarrow N_1 \bar{\nu}$ [63]. For heavy neutrino masses in the range of 100 – 300 GeV, this setup is projected to probe the mixing angles $|U_{eN}|^2$ and $|U_{\mu N}|^2$ with sensitivities up to two orders of magnitude beyond current bounds from electroweak precision data.

4.2 Boltzmann equations

We solve the full set of Boltzmann equations, including all relevant interactions, to track the evolution of the dark sector particles χ, ϕ as well as the heavy right-handed neutrinos. All relevant Feynman diagrams for these processes are collected in Appendix G.

As discussed in Section 3, under the assumption $m_\chi < m_\phi$, χ is the dark matter candidate. The field ϕ either decays completely before BBN or, in the freeze-in scenario, can also serve as a dark matter candidate. The yield of χ can achieve the observed relic abundance through either freeze-out or freeze-in processes.

The relevant collision terms $\mathcal{C}_\chi, \mathcal{C}_\phi, \mathcal{C}_{N_i}$ are

$$\begin{aligned}
\mathcal{C}_\chi = & \sum_{i,j=1}^6 \left[Y_{\mathbb{V}_i} Y_{\mathbb{V}_j} \langle \sigma v \rangle_{\mathbb{V}_i \mathbb{V}_j \rightarrow \chi \bar{\chi}} - Y_\chi^2 \langle \sigma v \rangle_{\chi \bar{\chi} \rightarrow \mathbb{V}_i \mathbb{V}_j} \right. \\
& + 2 \left(Y_h Y_{\mathbb{V}_i} \langle \sigma v \rangle_{h \mathbb{V}_i \rightarrow \chi \phi} - Y_\chi Y_\phi \langle \sigma v \rangle_{\chi \phi \rightarrow h \mathbb{V}_i} \right) + (h \leftrightarrow Z) \\
& + \theta(m_\phi - m_\chi - m_i) \left(\frac{1}{s} Y_\phi \langle \Gamma \rangle_{\phi \rightarrow \bar{\chi} \mathbb{V}_i} - Y_\chi Y_{\mathbb{V}_i} \langle \sigma v \rangle_{\bar{\chi} \mathbb{V}_i \rightarrow \phi} \right) \Big] \\
& + 2 \sum_{i=1}^3 \left(Y_W Y_{\ell_i} \langle \sigma v \rangle_{W \ell_i \rightarrow \chi \phi} - Y_\chi Y_\phi \langle \sigma v \rangle_{\chi \phi \rightarrow W \ell_i} \right) \\
& + \sum_{i=4}^6 \theta(m_\phi - m_\chi - m_i) \left(\frac{1}{s} Y_{\mathbb{V}_i} \langle \Gamma \rangle_{\mathbb{V}_i \rightarrow \chi \phi} - Y_\chi Y_\phi \langle \sigma v \rangle_{\chi \phi \rightarrow \mathbb{V}_i} \right) \\
& + Y_\phi^2 \left(2 \langle \sigma v \rangle_{\phi \phi \rightarrow \bar{\chi} \bar{\chi}} + \langle \sigma v \rangle_{\phi \bar{\phi} \rightarrow \chi \bar{\chi}} \right) - Y_\chi^2 \left(2 \langle \sigma v \rangle_{\bar{\chi} \bar{\chi} \rightarrow \phi \phi} + \langle \sigma v \rangle_{\chi \bar{\chi} \rightarrow \phi \bar{\phi}} \right), \tag{41}
\end{aligned}$$

$$\begin{aligned}
\mathcal{C}_\phi = & \sum_{i,j=1}^6 \left[Y_{\mathbb{V}_i} Y_{\mathbb{V}_j} \langle \sigma v \rangle_{\mathbb{V}_i \mathbb{V}_j \rightarrow \phi \bar{\phi}} - Y_\phi^2 \langle \sigma v \rangle_{\phi \bar{\phi} \rightarrow \mathbb{V}_i \mathbb{V}_j} \right. \\
& + 2 \left(Y_h Y_{\mathbb{V}_i} \langle \sigma v \rangle_{h \mathbb{V}_i \rightarrow \chi \phi} - Y_\chi Y_\phi \langle \sigma v \rangle_{\chi \phi \rightarrow h \mathbb{V}_i} \right) + (h \leftrightarrow Z) \\
& + \theta(m_\phi - m_\chi - m_i) \left(-\frac{1}{s} Y_\phi \langle \Gamma \rangle_{\phi \rightarrow \bar{\chi} \mathbb{V}_i} + Y_\chi Y_{\mathbb{V}_i} \langle \sigma v \rangle_{\bar{\chi} \mathbb{V}_i \rightarrow \phi} \right) \Big] \\
& + 2 \sum_{i=1}^3 \left(Y_W Y_{\ell_i} \langle \sigma v \rangle_{W \ell_i \rightarrow \chi \phi} - Y_\chi Y_\phi \langle \sigma v \rangle_{\chi \phi \rightarrow W \ell_i} \right) \\
& + \sum_{i=4}^6 \theta(m_i - m_\chi - m_\phi) \left(\frac{1}{s} Y_{\mathbb{V}_i} \langle \Gamma \rangle_{\mathbb{V}_i \rightarrow \chi \phi} - Y_\chi Y_\phi \langle \sigma v \rangle_{\chi \phi \rightarrow \mathbb{V}_i} \right) \\
& - Y_\phi^2 \left(2 \langle \sigma v \rangle_{\phi \phi \rightarrow \bar{\chi} \bar{\chi}} + \langle \sigma v \rangle_{\phi \bar{\phi} \rightarrow \chi \bar{\chi}} \right) + Y_\chi^2 \left(2 \langle \sigma v \rangle_{\bar{\chi} \bar{\chi} \rightarrow \phi \phi} + \langle \sigma v \rangle_{\chi \bar{\chi} \rightarrow \phi \bar{\phi}} \right), \tag{42}
\end{aligned}$$

$$\mathcal{C}_{N_i} = \sum_{i,j=1}^3 \left[k_{ij} \left(Y_\chi^2 \langle \sigma v \rangle_{\chi \bar{\chi} \rightarrow N_i N_j} + Y_\phi^2 \langle \sigma v \rangle_{\phi \bar{\phi} \rightarrow N_i N_j} \right) \right]$$

$$\begin{aligned}
& - k_{ij} Y_{\mathbb{N}_i} Y_{\mathbb{N}_j} \left(\langle \sigma v \rangle_{\mathbb{N}_i \mathbb{N}_j \rightarrow \chi \bar{\chi}} + \langle \sigma v \rangle_{\mathbb{N}_i \mathbb{N}_j \rightarrow \phi \bar{\phi}} \right) \\
& + 2 \left(Y_\chi Y_\phi \langle \sigma v \rangle_{\chi \phi \rightarrow h \mathbb{N}_i} - Y_h Y_{\mathbb{N}_i} \langle \sigma v \rangle_{h \mathbb{N}_i \rightarrow \chi \phi} \right) + 2(h \leftrightarrow Z) \\
& + 2 \theta(M_i - m_\chi - m_\phi) \left(-\frac{1}{s} Y_{\mathbb{N}_i} \langle \Gamma \rangle_{\mathbb{N}_i \rightarrow \chi \phi} + Y_\chi Y_\phi \langle \sigma v \rangle_{\chi \phi \rightarrow \mathbb{N}_i} \right) \\
& + 2 \theta(m_\phi - m_\chi - M_i) \left(\frac{1}{s} Y_\phi \langle \Gamma \rangle_{\phi \rightarrow \bar{\chi} \mathbb{N}_i} - Y_\chi Y_{\mathbb{N}_i} \langle \sigma v \rangle_{\bar{\chi} \mathbb{N}_i \rightarrow \phi} \right) \\
& + 2 \theta(M_i - m_W - m_{\ell_j}) \left(-\frac{1}{s} Y_{\mathbb{N}_i} \langle \Gamma \rangle_{\mathbb{N}_i \rightarrow W \ell_j} + Y_W Y_{\ell_j} \langle \sigma v \rangle_{W \ell_j \rightarrow \mathbb{N}_i} \right) \\
& + 2 \theta(M_i - m_h - m_j) \left(-\frac{1}{s} Y_{\mathbb{N}_i} \langle \Gamma \rangle_{\mathbb{N}_i \rightarrow h \nu_j} + Y_h Y_{\nu_j} \langle \sigma v \rangle_{h \nu_j \rightarrow \mathbb{N}_i} \right) + (h \leftrightarrow Z) \Big], \quad (43)
\end{aligned}$$

where $k_{ij} = 1$ (for $i \neq j$), $k_{ij} = 2$ (for $i = j$).

In the first two collision terms, we introduce the notation $\mathbb{V}_{4,5,6} \equiv \mathbb{N}_{1,2,3}$ and $m_{4,5,6} \equiv M_{1,2,3}$ for simplicity. The theta functions indicate whether the decay and inverse annihilation processes are kinematically allowed. For processes involving solely SM particles in either initial or final states, it is more convenient to compute the evolution via the inverse processes. For example, it is easier to evaluate the term $[(Y_\chi^{\text{eq}})^2 - Y_\chi^2] \langle \sigma v \rangle_{\chi \bar{\chi} \rightarrow \nu_i \nu_j}$ than $(Y_{\nu_i} Y_{\nu_j} \langle \sigma v \rangle_{\nu_i \nu_j \rightarrow \chi \bar{\chi}} - Y_\chi^2 \langle \sigma v \rangle_{\chi \bar{\chi} \rightarrow \nu_i \nu_j})$.

Discussion about coefficients in the Boltzmann equations In the collision terms, the coefficient ± 2 in front of certain contributions indicate that two units of particle are created or annihilated. The squared amplitude should have an overall factor of $1/2$ that accounts for avoiding double counting when integrating over the phase space of two identical particles, which is however absorbed into the definition of the cross-section for the given process. Hence, at the Boltzmann equation level, the $1/2$ accounted for identical particles does not show up.

The factor discussed above also appears in processes involving the Majorana neutrinos. For example, both $\mathbb{N}_i \leftrightarrow \chi \phi$ and its conjugate channel $\mathbb{N}_i \leftrightarrow \bar{\chi} \bar{\phi}$ contribute to the same collision term, yielding an overall factor of 2 in $dY_{\mathbb{N}_i}/dT$. In contrast, χ and $\bar{\chi}$ (and similarly ϕ and $\bar{\phi}$) are treated as symmetric but distinct species with $Y_\chi = Y_{\bar{\chi}}$ and $Y_\phi = Y_{\bar{\phi}}$, so each channel contributes to its own species and no extra factor 2 appears in the Boltzmann equations for Y_χ and Y_ϕ . The same reason applies to other channels such as $\phi \leftrightarrow \bar{\chi} \mathbb{N}_i$ ($\bar{\phi} \leftrightarrow \chi \mathbb{N}_i$) and $\chi \phi (\bar{\chi} \bar{\phi}) \rightarrow Z \mathbb{N}_i$. For the processes $\chi \phi \leftrightarrow h \mathbb{N}_i$, it contains four related channels: $\chi \phi, \bar{\chi} \bar{\phi} \leftrightarrow LH, \bar{L} \bar{H}$. The factor 2 in front of $W \ell_i \leftrightarrow \chi \phi$ arises from $W^+ \ell_i^-$ and $W^- \ell_i^+$.

The total relic abundance of dark matter is obtained by combining the contributions from χ and $\bar{\chi}$, i.e., $2Y_\chi$, and ϕ and $\bar{\phi}$ ($2Y_\phi$) if they are also dark matter candidates.

Boltzmann equations for freeze-out and freeze-in The evolution of all dark sector particles is governed by the coupled Boltzmann equations for comoving number densities $Y_\chi, Y_\phi, Y_{\mathbb{N}_i}$. For the **freeze-out evolution**,

$$\frac{dY_\chi}{dT} = -\frac{s}{T\bar{H}} \mathcal{C}_\chi, \quad (44)$$

$$\frac{dY_\phi}{dT} = -\frac{s}{T\bar{H}} \mathcal{C}_\phi, \quad (45)$$

$$\frac{dY_{\mathbb{N}_i}}{dT} = -\frac{s}{T\bar{H}} \mathcal{C}_{\mathbb{N}_i}, \quad (46)$$

where the entropy density is given by $s = \frac{2\pi^2}{45} h_{\text{eff}} T^3$, and

$$\bar{H} = \frac{H}{1 + \frac{1}{3} \frac{T}{h_{\text{eff}}} \frac{dh_{\text{eff}}}{dT}} = \sqrt{\frac{\pi^2 g_{\text{eff}}}{90}} \frac{T^2/M_{\text{Pl}}}{1 + \frac{1}{3} \frac{T}{h_{\text{eff}}} \frac{dh_{\text{eff}}}{dT}}. \quad (47)$$

For the **freeze-in evolution**, if the hidden sector interactions are strong enough to maintain internal thermal equilibrium, one can introduce a hidden sector temperature T_h defined via the hidden sector energy density [33]. The coupled Boltzmann equations for Y_χ , Y_ϕ , $Y_{\mathbb{N}_i}$ and the temperature ratio $\eta \equiv T_v/T_h$ are

$$\frac{dY_\chi}{dT} = -\frac{s}{H} \frac{d\rho_h/dT_h}{4\rho_h - j_h/H} \mathcal{C}_\chi, \quad (48)$$

$$\frac{dY_\phi}{dT} = -\frac{s}{H} \frac{d\rho_h/dT_h}{4\rho_h - j_h/H} \mathcal{C}_\phi, \quad (49)$$

$$\frac{dY_{\mathbb{N}_i}}{dT} = -\frac{s}{H} \frac{d\rho_h/dT_h}{4\rho_h - j_h/H} \mathcal{C}_{\mathbb{N}_i}, \quad (50)$$

$$\frac{d\eta}{dT_h} = -\frac{A_v}{B_v} + \frac{\rho_v + j_h/(4H)}{\rho_h - j_h/(4H)} \frac{d\rho_h}{dT_h}, \quad (51)$$

where A_v and B_v can be found in Appendix H, and the energy transfer density is given by

$$\begin{aligned} j_h = & \sum_{i,j=1}^3 \left[2\theta(m_\phi - m_\chi - m_i) \left(-Y_\phi s J_{\phi \rightarrow \bar{\chi} \nu_i} + Y_\chi Y_{\nu_i} s^2 J_{\bar{\chi} \nu_i \rightarrow \phi} \right) \right. \\ & + \theta(M_i - m_W - m_{\ell_j}) \left(-Y_{\mathbb{N}_i} s J_{\mathbb{N}_i \rightarrow W \ell_j} + Y_W Y_{\ell_j} s^2 J_{W \ell_j \rightarrow \mathbb{N}_i} \right) \\ & + 2\theta(M_i - m_h - m_j) \left(-Y_{\mathbb{N}_i} s J_{\mathbb{N}_i \rightarrow h \nu_j} + Y_h Y_{\nu_j} s^2 J_{h \nu_j \rightarrow \mathbb{N}_i} \right) + (h \leftrightarrow Z) \\ & + 2 \left(Y_h Y_{\nu_i} s^2 J_{h \nu_i \rightarrow \chi \phi} - Y_\chi Y_\phi s^2 J_{\chi \phi \rightarrow h \nu_i} \right) + 2(h \leftrightarrow Z) \\ & \left. + 4 \left(Y_W Y_{\ell_i} s^2 J_{W \ell_i \rightarrow \chi \phi} - Y_\chi Y_\phi s^2 J_{\chi \phi \rightarrow W \ell_i} \right) \right]. \quad (52) \end{aligned}$$

The evolution of dark particles χ, ϕ as well as the right-handed neutrinos \mathbb{N}_i is computed using the coupled Boltzmann equations above, and the results are presented in the following subsection.

If hidden sector interactions, such as $\chi \bar{\chi} \leftrightarrow \phi \bar{\phi}$, are too weak to establish internal equilibrium, their effects on the dark matter relic density can be safely neglected. In this regime, the freeze-in production of dark matter can be computed using a two-step procedure: (1) first determine the freeze-in production of χ and ϕ from SM particles, assuming that ϕ does not interact with χ ; (2) if ϕ can decay into χ , then include its contribution by calculating the decay of ϕ after the freeze-in production has completed.

However, this treatment is not appropriate when the hidden sector possesses sufficiently strong internal interactions and can thus maintain thermal equilibrium. In such cases, the resulting error can be as large as 30%, as shown by explicit comparison.

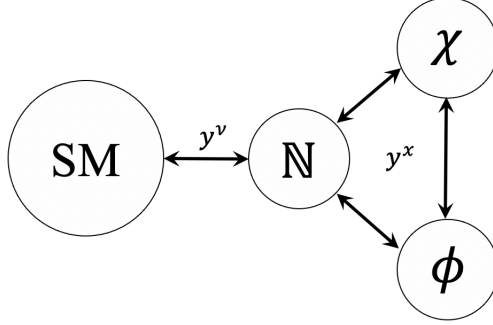


Figure 4: A schematic illustration of the dark sector evolution via freeze-out. At high temperatures, the dark particles χ and ϕ remain in thermal equilibrium with the SM plasma through the right-handed neutrino portal. The dominant freeze-out channels are $\chi\bar{\chi}, \phi\bar{\phi} \rightarrow \mathbb{N}\mathbb{N}$, and \mathbb{N} subsequently decays into SM particles.

4.3 Evolution of the benchmark models

Using the PSO algorithm described in Section 2.3.4, we determine seesaw parameter sets for all three cases (Case-RS, SC, SS), yielding five representative benchmark models that reproduce the observed neutrino mass hierarchy and mixing, as listed in Appendix I.

4.3.1 Freeze-out evolution, Case-RS, SC

The freeze-out scenario is illustrated schematically in Fig. 4, where the dark sector particles χ and ϕ maintain thermal equilibrium with the SM sector via the right-handed neutrinos. The dark particles χ and ϕ annihilate efficiently into pairs of right-handed neutrinos, which subsequently decay into SM particles. In this paper we assume that ϕ is heavier than the dark matter candidate χ , and that ϕ eventually decays completely before BBN. For the freeze-out scenario, we investigate five representative benchmark models for Case-RS and SC, presented in Table 1. Parameters are chosen to satisfy all current experimental constraints, shown in Section 4.1, as well as the observed abundance of the dark matter.

Freeze-out	Benchmark	m_χ	m_ϕ	$y_{1,2,3}^x$	$\Omega_\chi h^2$	τ_ϕ [sec]
Model <i>a</i>	RS	210	350	0.433	0.12	1.26×10^{-12}
Model <i>b</i>		210	420	0.516	0.12	1.45×10^{-23}
Model <i>c</i>	SC	210	350	0.515	0.12	5.76×10^{-22}
Model <i>d</i>		210	420	0.620	0.12	1.00×10^{-23}
Model <i>e</i>		120	130	0.084	0.12	1.09×10^{-18}

Table 1: Freeze-out benchmark models we discuss in this work for Case-RS and SC. All masses are in the unit of GeVs. The lifetimes of ϕ (τ_ϕ) and right-handed neutrinos $\mathbb{N}_{1,2,3}$ for each model are ensured to be less than one second. The dark fermion χ serves as the dark matter candidate with a full occupation of the observed dark matter relic density. For simplicity, we set the values of coupling $y_{1,2,3}^x$ to be the same. The lifetimes of ϕ in seconds are listed in the last column for the five models.

Case-RS freeze-out evolution For Model *a* taking the Benchmark-RS seesaw parameters, the evolution is shown in Fig. 5 (a). Owing to the mass hierarchy $m_\chi > M_1$, the dominant process depleting dark matter χ is the secluded channel $\chi\bar{\chi} \rightarrow \mathbb{N}_1\mathbb{N}_1$. In this case the couplings between the hidden and visible sectors are relatively weak, so the portal neutrinos \mathbb{N}_i mainly decrease through interactions $\mathbb{N}_i\mathbb{N}_j \rightarrow \chi\bar{\chi}$ ($i, j = 1, 2, 3$) for $M_i + M_j > 2m_\chi$, which simultaneously act as a production channel for χ . At the same time, \mathbb{N}_i decay to SM particles via $\mathbb{N}_i \rightarrow W^\pm\ell_j^\mp$, with subdominant channels $\mathbb{N}_i \rightarrow h\nu_j, Z\nu_j$ being suppressed by the tiny Yukawa couplings or neutrino mixing. All right-handed neutrinos eventually decrease to zero. For the particle ϕ , the dominant interactions are $\phi\phi \rightarrow \bar{\chi}\chi$, $\phi\bar{\phi} \rightarrow \chi\bar{\chi}$, and $\phi\bar{\phi} \rightarrow \mathbb{N}_i\mathbb{N}_j$. Dark particle annihilation through $\chi\phi \rightarrow LH$ plays only a subdominant role. At later times, all remaining ϕ decay through $\phi \rightarrow \bar{\chi}\nu_i$ before BBN.

The evolution for Model *b* is shown in Fig. 5 (b). In this case, the scalar mass m_ϕ is raised such that $m_\phi > (m_\chi + M_1)$, which opens an efficient decay channel $\phi \rightarrow \bar{\chi}\mathbb{N}_1$ together with its inverse process. Since the decay of ϕ generates a substantial number of χ , a relatively large value of $y_{1,2,3}^x$ is required to prevent the overproduction of dark matter through the channel $\chi\bar{\chi} \rightarrow \mathbb{N}_1\mathbb{N}_1$. The portal neutrinos can deplete via internal interactions $\mathbb{N}_i\mathbb{N}_j \rightarrow \chi\bar{\chi}$, and can decay into SM particles via $\mathbb{N}_i \rightarrow W^\pm\ell_j^\mp, h\nu_j, Z\nu_j$, similar to Model *a*. With a suitable choice of parameters, the abundance of the dark fermion χ eventually reaches the observed dark matter relic density, while other dark particles are depleted to negligible levels before BBN.

Case-SC freeze-out evolution For Case-SC, the sizable Yukawa couplings y_{ij} (Table I) together with neutrino mixing elements $|U_{ij}|$ (Table I) ensure an initial thermal equilibrium between two sectors. The evolution of Model *c* taking the Benchmark-SC seesaw parameters is plotted in Fig. 5 (c), where the portal neutrinos \mathbb{N}_i remain closely coupled to the thermal bath, giving rise to a delayed freeze-out compared to the previous models. The evolution is similar to Model *a*, in which χ predominately annihilate through $\chi\bar{\chi} \rightarrow \mathbb{N}_1\mathbb{N}_1$, and processes $\mathbb{N}_i\mathbb{N}_j \rightarrow \chi\bar{\chi}$, $\phi\phi \rightarrow \bar{\chi}\chi$, and $\phi\bar{\phi} \rightarrow \chi\bar{\chi}$ proceed simultaneously. ϕ can annihilate via $\phi\phi \rightarrow \bar{\chi}\chi$, $\phi\bar{\phi} \rightarrow \chi\bar{\chi}$, $\phi\bar{\phi} \rightarrow \mathbb{N}_i\mathbb{N}_j$, and after ϕ freezes out, it also decays completely via $\phi \rightarrow \bar{\chi}, \nu_i$ before BBN. The dark particle annihilation channel $\chi\phi \rightarrow LH$ is phenomenologically negligible.

Model *e* satisfies $M_3 > (m_\chi + m_\phi)$, which allows the decay channel $\mathbb{N}_3 \rightarrow \chi\phi, \bar{\chi}\bar{\phi}$ along with the corresponding inverse annihilations. In this case, the dark particle annihilation channels $\chi\bar{\chi}, \phi\bar{\phi} \rightarrow \mathbb{N}_i\mathbb{N}_j$ are suppressed, and the dominant freeze-out process for the dark particles is $\chi\phi \rightarrow LH$. Interactions of \mathbb{N}_3 within the dark sector dominate over its SM channels, leading to an eventual decoupling of \mathbb{N}_3 from the thermal bath. The right-handed neutrinos \mathbb{N}_1 and \mathbb{N}_2 tightly couple to the SM sector through three-point interactions $\mathbb{N}_i \leftrightarrow W^\pm\ell_j^\mp, h\nu_j, Z\nu_j$. The particles χ and ϕ interact with each other via $\phi\phi \leftrightarrow \bar{\chi}\chi$ and $\phi\bar{\phi} \leftrightarrow \chi\bar{\chi}$, mediated by the neutrinos ν_{1-6} . Their abundances are further depleted by several channels including $\chi\bar{\chi} \rightarrow \nu_i\nu_j, \chi\phi \rightarrow h\nu_i, Z\nu_i, Wl$, and $\phi \leftrightarrow \bar{\chi}\nu_i$. Ultimately, the abundance of ϕ drops down to negligible level before BBN, while χ attains the observed dark matter relic abundance.

4.3.2 Freeze-in evolution, Case-RS, SC, SS

The freeze-in scenario is illustrated schematically in Figs. 6 and 7. There are two distinct possibilities, depending on whether the right-handed neutrinos can reach thermal equilibrium

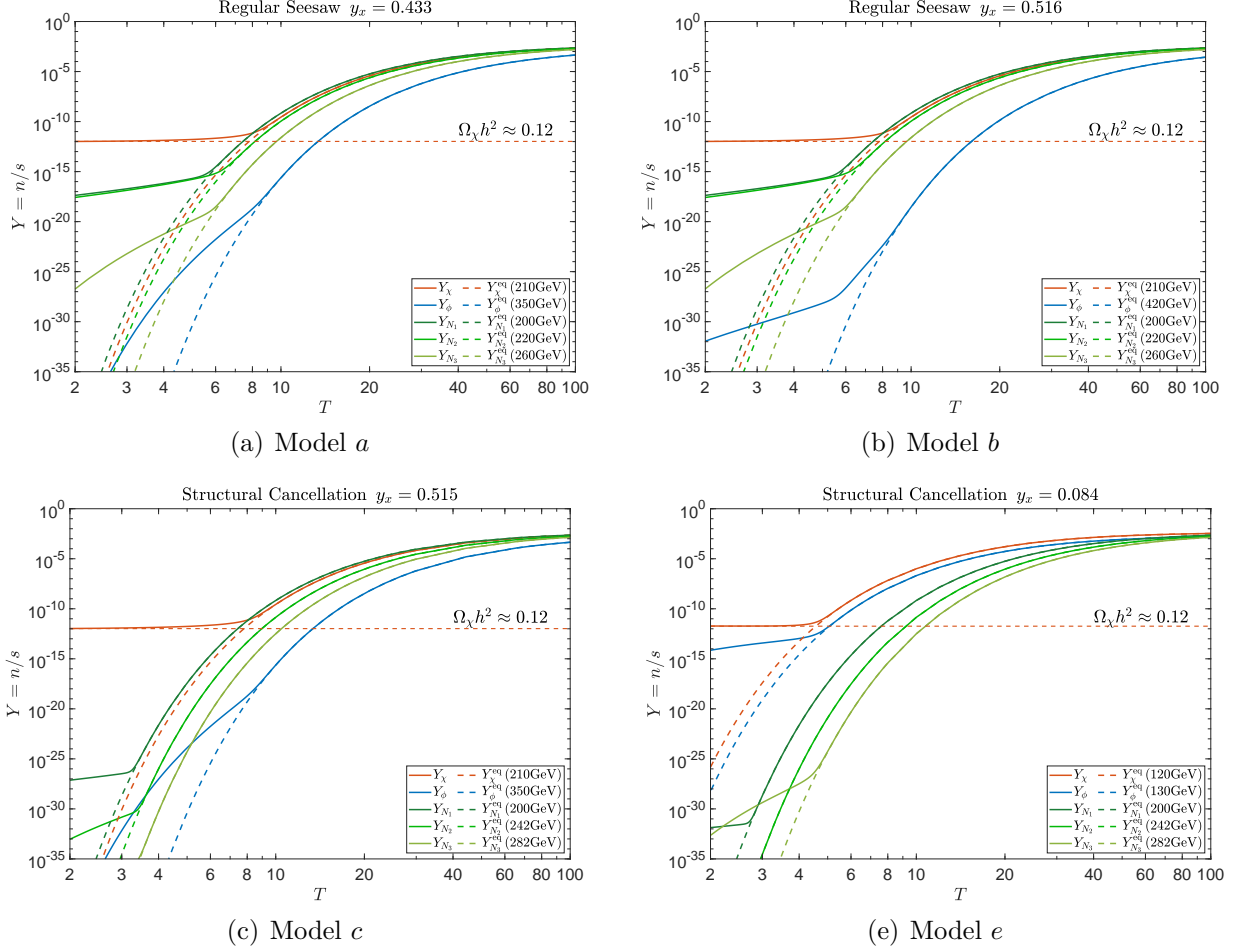


Figure 5: An exhibition of the dark sector freeze-out evolution for Models a, b (Benchmark-RS) and Models c, e (Benchmark-SC). For each model, the figure shows the evolution of the comoving number densities of all dark particles χ, ϕ , and $\mathbb{N}_{1,2,3}$, where the dark fermion χ serves as the dark matter candidate. The red horizontal dashed line indicates the observed dark matter relic density with dark matter mass equal to m_χ . For Benchmark-RS, the difference between two models is as follows. In Model a , ϕ freezes out via $\phi\bar{\phi} \rightarrow \mathbb{N}_{1,2,3}\mathbb{N}_{1,2,3}$ and annihilates into χ through $\phi\phi \rightarrow \bar{\chi}\chi$, $\phi\bar{\phi} \rightarrow \chi\bar{\chi}$. At later times, all remaining ϕ decay through $\phi \rightarrow \bar{\chi}\mathbb{V}_{1,2,3}$ before BBN. While in Model b , the mass hierarchy $m_\phi > (m_\chi + M_1)$ allows the internal decay channel $\phi \rightarrow \bar{\chi}\mathbb{N}_1$. For Benchmark-SC, the portal neutrinos $\mathbb{N}_{1,2,3}$ remain tightly coupled to the thermal bath, leading to a delayed freeze-out. In Model e , \mathbb{N}_3 decays via $\mathbb{N}_3 \rightarrow \chi\phi, \bar{\chi}\bar{\phi}$, and the dominant freeze-out channel for dark particles is $\chi\phi \rightarrow LH$.

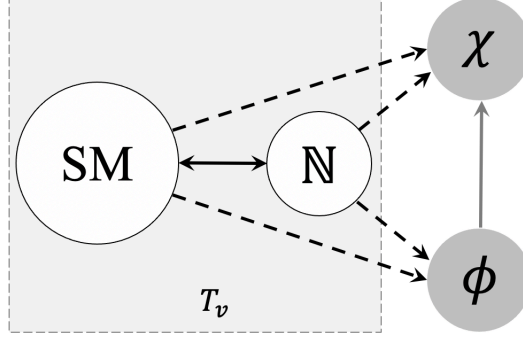


Figure 6: For Case-RS and SC, the right-handed neutrinos reach thermal equilibrium during the main freeze-in epoch of the dark particles and can thus be treated as part of the visible sector, sharing the visible sector temperature. A consistent model further requires that ϕ decay completely before BBN, so the corresponding coupling y^x is not large enough to maintain internal thermal equilibrium within the dark sector. Hence, the dark particles are produced via freeze-in through the processes $\mathbb{N}\mathbb{N} \rightarrow \chi\bar{\chi}$, $\phi\bar{\phi}$ and $LH \rightarrow \chi\phi$.

with the SM sector.

Seen from Eq. (35), after including the seesaw mixing, ϕ can decay into χ and a light neutrino via $\phi \rightarrow \bar{\chi} + \mathbb{V}$, with an effective coupling constant

$$y_i^{x'} \sim y_i^x U_{\mathbb{N}\mathbb{V}}, \quad (53)$$

where $U_{\mathbb{N}\mathbb{V}}$ is the seesaw mixing between light and heavy neutrinos in the mass eigenstate basis, as defined in Eqs. (8) and (9).

For χ and ϕ masses of order a few hundred GeV, the scalar ϕ decays before BBN if $y_i^{x'} \gtrsim 10^{-12}$, whereas its lifetime exceeds the age of the Universe for $y_i^{x'} \lesssim 10^{-22}$.

Case-RS freeze-in In Case-RS, the electroweak right-handed neutrinos have Yukawa couplings of order $y^\nu \sim 10^{-7}$, resulting in a seesaw mixing $U_{\mathbb{N}\mathbb{V}} \sim 10^{-8} - 10^{-7}$. These electroweak right-handed neutrinos reach thermal equilibrium with the SM particles below the TeV scale. There are two cases:

1. Both χ, ϕ are DM. The requirement of $y_i^{x'} \lesssim 10^{-22}$ gives rise to $y_i^x \lesssim 10^{-15} - 10^{-14}$.
 - For $M_N > m_\chi + m_\phi$, the major freeze-in process is $\mathbb{N} \rightarrow \chi + \phi$. Given $y^x \sim 10^{-15} - 10^{-14}$, the freeze-in production is not sufficient. **X**
 - For $M_N < m_\chi + m_\phi$, the freeze-in processes are $\mathbb{N}\mathbb{N} \rightarrow \chi\bar{\chi}$ and $\mathbb{N}\mathbb{N} \rightarrow \phi\bar{\phi}$. The four-point freeze-in production is less efficient compared to the decaying process in the previous case. The contribution from the other freeze-in process $LH \rightarrow \chi\phi$ is even more suppressed. **X**
2. Only χ is DM. In this case ϕ decays before BBN, thus $y_i^{x'} \gtrsim 10^{-12}$ requires $y^x \gtrsim 10^{-6} - 10^{-7}$:

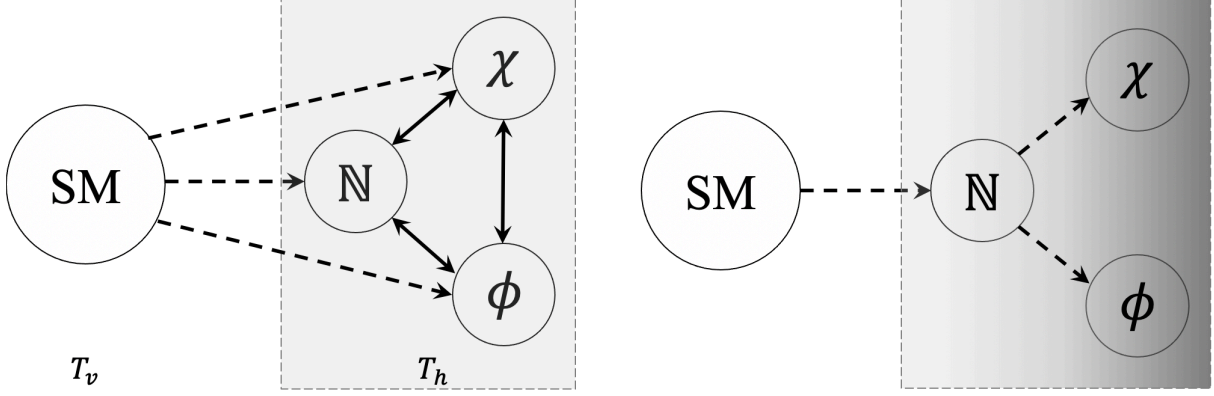


Figure 7: For Case-SS, the portal right-handed neutrino \mathbb{N}_1 couples ultraweakly to the SM and therefore never reaches thermal equilibrium with it. Depending on the value of y^x , the dark sector can either reach internal equilibrium (left panel), in which case one can define a hidden sector temperature T_h (Model *d*), or remain out of internal equilibrium (right panel), in which case both χ and ϕ are dark matter candidates (Model *e*).

- For $M_N > m_\chi + m_\phi$, the major freeze-in process is $\mathbb{N} \rightarrow \chi + \phi$. Given $y_x \gtrsim 10^{-6} - 10^{-7}$, the freeze-in production is too large, resulting in an overproduction of dark matter. **✗**
- For $M_N < m_\chi + m_\phi$, the freeze-in processes are $\mathbb{N}\mathbb{N} \rightarrow \chi\bar{\chi}$, $\mathbb{N}\mathbb{N} \rightarrow \phi\bar{\phi}$, and $LH \rightarrow \chi\phi$. Freeze-in models *a, b* for Benchmark RS are shown in Table 2. **✓**

Case-SC freeze-in In Case-SC, the electroweak right-handed neutrinos have Yukawa couplings of order $y' \sim 0.01 - 0.1$, resulting in a seesaw mixing $U_{\mathbb{N}\nu} \sim 0.01$. These electroweak right-handed neutrinos remain in thermal equilibrium with the SM particles. There are also two cases:

1. Both χ, ϕ are DM. The requirement $y_i^{x'} \lesssim 10^{-22}$ implies $y_i^x \lesssim 10^{-20}$, which is far too small to generate a significant freeze-in abundance. **✗**
2. Only χ is DM. In this case $y_i^{x'} \gtrsim 10^{-12}$ then requires $y^x \gtrsim 10^{-10}$.
 - For $M_N > m_\chi + m_\phi$, the dominant freeze-in process is $\mathbb{N} \rightarrow \chi + \phi$, which leads to an overproduction of dark matter via freeze-in. **✗**
 - For $M_N < m_\chi + m_\phi$, the freeze-in processes are $\mathbb{N}\mathbb{N} \rightarrow \chi\bar{\chi}$, $\mathbb{N}\mathbb{N} \rightarrow \phi\bar{\phi}$, and $LH \rightarrow \chi\phi$. Freeze-in model *c* for Benchmark SC is shown in Table 2. **✓**

The freeze-in production of dark matter for Case-RS and SC is illustrated schematically in Fig. 6. During the main freeze-in epoch ($T \sim m_{\text{DM}}$), the right-handed neutrinos are in thermal equilibrium with the SM sector. However, as discussed above, the dark sector coupling y^x is not large enough, so the internal dark sector interactions are too weak to establish thermal equilibrium within the dark sector.

Case-SS freeze-in In Case-SS, one of the electroweak right-handed neutrinos (taken to be \mathbb{N}_1) has a Yukawa coupling much smaller than the typical seesaw coupling, $y^\nu \ll 10^{-7}$, resulting in the seesaw mixing $U_{\mathbb{N}_1\nu} \lesssim 10^{-10}$ for \mathbb{N}_1 . Because of this feeble interaction, \mathbb{N}_1 never reaches thermal equilibrium with the SM bath. Consequently, dark matter can only be produced via freeze-in through the \mathbb{N}_1 portal. There are also two cases:

1. Both χ and ϕ are dark matter. The requirement $y_i^{x'} \lesssim 10^{-22}$ implies $y_i^x \lesssim 10^{-22}/y^\nu$, which typically yields $y_i^x \lesssim 10^{-10}$. Such a tiny coupling prevents the dark sector from reaching thermal equilibrium. In this case, the observed dark matter relic abundance can only be obtained if $M_N > m_\chi + m_\phi$. ✓
2. In this case only χ constitutes dark matter. The coupling y_1^x must be sufficiently large so that $y_i^{x'} \sim y_1^x U_{\mathbb{N}_1\nu} \sim 10^{-12}$, which implies $y_1^x \gtrsim 0.1$. Depending on the precise values of y_1^x and dark particle masses, the dark sector may or may not reach internal thermal equilibrium. In the former case one can consistently define a hidden sector temperature, whereas in the latter case the dark sector remains out of equilibrium throughout the freeze-in process. ✓

The freeze-in production of dark matter for Case-SS is illustrated in Fig. 7. In this case, the portal right-handed neutrino never reaches thermal equilibrium with the SM sector. Depending on the size of the dark sector coupling y^x , the dark sector may either attain internal thermal equilibrium or remain out of equilibrium throughout its evolution.

For the various cases discussed above, we compute the evolution of the dark sector particles and determine the resulting dark matter relic abundance, as summarized in Table 2. Models *d, e* are particularly interesting, since in these two cases the dark sector reaches internal thermal equilibrium; the evolution are shown in Fig. 8.

In Model *d* taking the Benchmark-SS1 seesaw parameters, dark particles χ, ϕ , and \mathbb{N}_1 are produced via freeze-in through the processes $LH \rightarrow \chi\phi$ and $LH \rightarrow \mathbb{N}_1$. Particles χ and ϕ interact through $\phi\phi \leftrightarrow \overline{\chi\chi}$ ($\phi\overline{\phi} \leftrightarrow \chi\chi$), and annihilate into \mathbb{N}_1 via $\chi\overline{\chi} \rightarrow \mathbb{N}_1\mathbb{N}_1$, $\phi\overline{\phi} \rightarrow \mathbb{N}_1\mathbb{N}_1$, causing Y_χ and Y_ϕ to decrease while $Y_{\mathbb{N}_1}$ increases. Later, once the thermally averaged decay rate of \mathbb{N}_1 exceeds the Hubble expansion rate, the decay $\mathbb{N}_1 \rightarrow LH$ becomes active and $Y_{\mathbb{N}_1}$ rapidly drops down to zero. Since $m_\phi > m_\chi$, the dark fermion χ accounts for the observed dark matter relic density, while ϕ eventually decays away at lower temperatures before BBN.

For this model, we take the opportunity to clarify a common misconception in the literature regarding the calculation of the dark matter relic density in such setups. In our treatment, we solve the full coupled evolution of the freeze-in dark matter χ together with all other dark sector particles ϕ and \mathbb{N}_1 that are produced via freeze-in, including all dark sector internal interactions, and we find $\Omega_\chi h^2 = 0.12$. By contrast, a common approximate procedure in the literature is to neglect all dark sector internal interactions, compute the freeze-in production of χ, ϕ , and \mathbb{N}_1 separately (assuming that ϕ and \mathbb{N}_1 do not decay during the freeze-in epoch), and then let ϕ and \mathbb{N}_1 decay completely after freeze-in, adding their contributions to the final χ relic density. In this case, since the right-handed neutrino \mathbb{N}_1 cannot decay into dark particles, the freeze-in contribution from $\mathbb{N}_1 \rightarrow \chi\phi$ is absent. As a result, the approximate treatment deviates strongly from our full calculation, which yields a dark matter relic density $\Omega_\chi h^2 = 0.004$, corresponding to an error exceeding 95%.

Freeze-in	Benchmark	m_χ	m_ϕ	y_1^x	$y_{2,3}^x$	$\Omega_\chi h^2$	$\Omega_\phi h^2$	τ_ϕ [sec]
Model <i>a</i>	RS	240	360	2.2×10^{-6}	2.2×10^{-6}	0.12	0	6.28×10^{-2}
Model <i>b</i>		100	330	2.8×10^{-6}	2.8×10^{-6}	0.12	0	7.75×10^{-14}
Model <i>c</i>	SC	180	400	1.6×10^{-10}	1.6×10^{-10}	0.12	0	5.39×10^{-5}
Model <i>d</i>	SS1	440	450	0.29	—	0.12	0	9.00×10^{-2}
Model <i>e</i>	SS2	120	200	0.90	—	0.12	0	0.92
Model <i>f</i>	SS3	90	100	1.7×10^{-12}	—	0.057	0.063	1.89×10^{19}

Table 2: Freeze-in benchmark models for Cases RS, SC, and SS, covering all viable configurations. All masses are given in GeV. In models (*a*–*d*) where only χ is dark matter, the dark fermion χ accounts for the entire observed dark matter relic abundance, and the lifetimes of ϕ and the right-handed neutrinos $\mathbb{N}_{1,2,3}$ are shorter than 1 sec, so that they decay completely before BBN for Models *a*–*e*. In model *f* where both χ and ϕ contribute to dark matter, the lifetime of ϕ exceeds the age of the Universe. In Case-SS we assume that only \mathbb{N}_1 , which couples minimally to the SM, serves as the portal to the dark sector. The difference between benchmarks SS1, SS2 and SS3 lies in the seesaw Yukawa coupling y_1^x , taken to be of order 10^{-11} and 10^{-13} , respectively, which in turn fixes the corresponding values of y_1^x .

In Model *e* taking the Benchmark-SS2 seesaw parameters, since $M_1 > m_\chi + m_\phi$, the three-point decay within the dark sector $\mathbb{N}_1 \rightarrow \chi\phi$ is kinematically allowed. Dark particles χ and ϕ then accumulate both by the freeze-in process $LH \rightarrow \chi\phi$ and by $LH \rightarrow \mathbb{N}_1$ followed by $\mathbb{N}_1 \rightarrow \chi\phi$. When the interaction rate of processes $\bar{\chi}\chi \rightarrow \phi\phi$ falls below the Hubble rate at $T_v \simeq 10^2$ GeV, this channel becomes inefficient, marking the onset of the dark freeze-out during which the number density of ϕ starts to decrease. The dark freeze-out ends once the reverse process $\phi\phi \rightarrow \bar{\chi}\chi$ becoming inactive, with its rate dropping below the Hubble scale. Afterwards, the abundance of ϕ gradually levels off and remains constant until ϕ eventually decay at low temperatures, with a lifetime shorter than 1 second. During the dark freeze-out, the dark matter χ continues to grow and ultimately attains the observed relic density. In this case, the eventually decrease of $Y_{\mathbb{N}_1}$ is driven by several effects, including $\mathbb{N}_1 \rightarrow \chi\phi$, $\mathbb{N}_1\mathbb{N}_1 \rightarrow \chi\bar{\chi}$, and $\mathbb{N}_1\mathbb{N}_1 \rightarrow \phi\bar{\phi}$.

The dark matter particle χ ultimately reaches the observed relic abundance $\Omega_\chi h^2 = 0.12$, once the full evolution of all dark sector particles is taken into account. Unlike in the previous case, the right-handed neutrino is heavier than $m_\chi + m_\phi$, so the decay of \mathbb{N}_1 makes a strong contribution to the dark matter freeze-in. The approximate procedure, where the freeze-in production of χ , ϕ , and \mathbb{N}_1 is computed separately and the contributions from the late decays of ϕ and \mathbb{N}_1 are added to the dark matter relic density after freeze-in, leads to a dark matter relic density $\Omega_\chi h^2 = 0.08$, corresponding to a 30% error.

In Model *f* taking the Benchmark-SS3 seesaw parameters, the tiny coupling $y_i^x \lesssim 10^{-10}$ prevents the dark sector from reaching internal thermal equilibrium. The decays $\phi \rightarrow \bar{\chi} + \mathbb{V}_{1,2,3}$ have lifetimes exceeding the age of the Universe. Both χ and ϕ are dark matter components that can only be produced via freeze-in through the \mathbb{N}_1 portal, and together they account for the entire dark matter relic density.

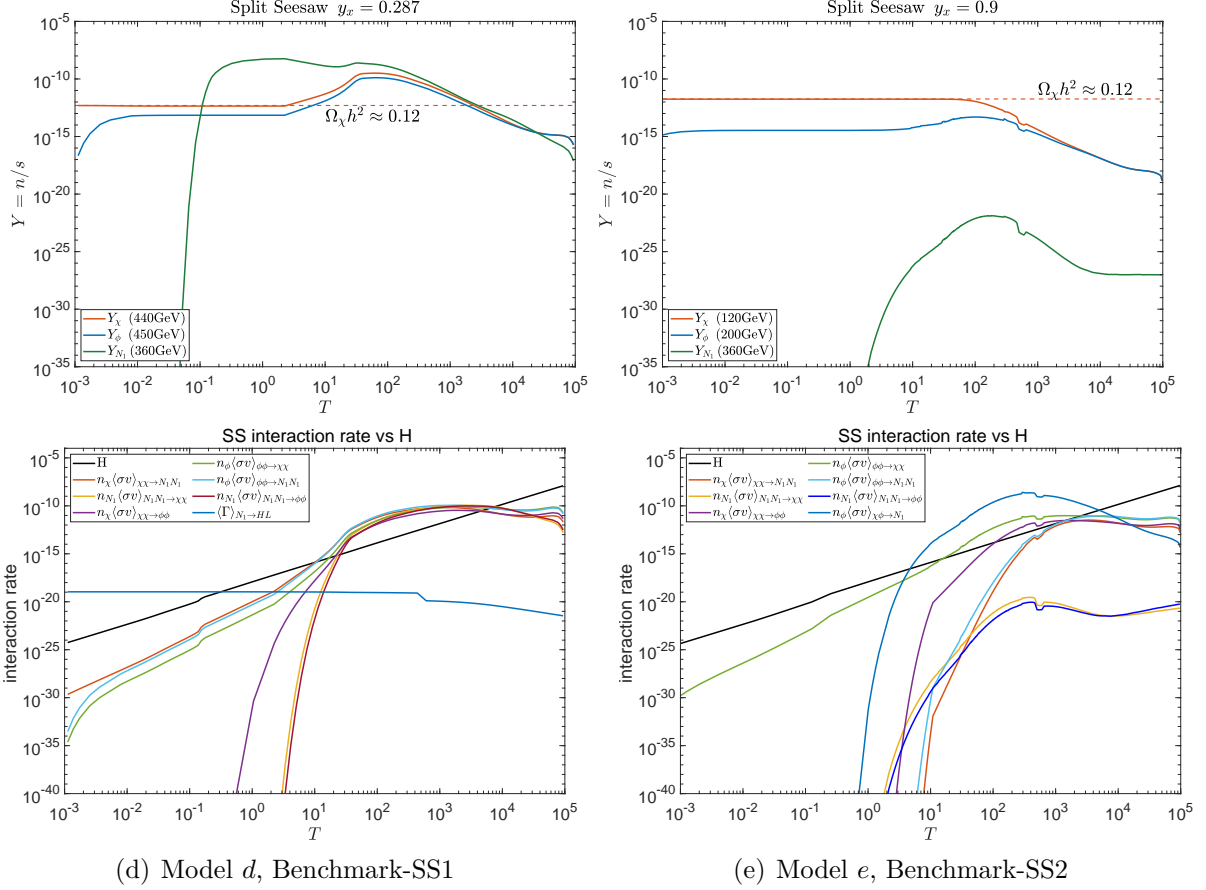


Figure 8: An exhibition of the freeze-in evolution for Model *d* (Benchmark-SS1) and Model *e* (Benchmark-SS2) in terms of the visible sector temperature T (GeV). The top panels show the evolution of the comoving number densities of dark particles χ , ϕ , and \mathbb{N}_1 , where the red horizontal dashed line denotes the observed dark matter relic density for a dark matter mass m_χ . In the lower figure, we trace the dark sector interaction rates compared to the Hubble rate. In both cases, the dark particles are produced via freeze-in processes $LH \rightarrow \chi\phi$ and $LH \rightarrow \mathbb{N}_1$, and the dark sector reaches internal thermal equilibrium once the relevant interaction rates exceed the Hubble. For Case-SS2, the decay channel $\mathbb{N}_1 \rightarrow \chi\phi$ is allowed because $M_1 > (m_\chi + m_\phi)$. All remaining ϕ and \mathbb{N}_1 decays completely with lifetimes shorter than 1 second.

5 Conclusion

In this work, we have explored electroweak scale implementations of the Type-I seesaw mechanism and their connection to dark matter via a right-handed neutrino portal. We have studied a minimal dark sector coupled to right-handed neutrinos and precisely carried out a detailed analysis of its cosmological evolution.

We began by emphasizing the central role of right-handed neutrinos in neutrino mass model building. As electroweak singlet fermions, their neutral nature allows Majorana mass terms, opens the door to leptogenesis, and makes them natural portal fields to hidden sectors. When their masses lie in electroweak to TeV scale, it is plausible that the origin of this mass scale is linked to electroweak symmetry breaking, and crucially, they become experimentally accessible at colliders and in precision neutrino experiments. In this mass range, constraints from colliders, electroweak precision tests, and flavor physics are significant but still leave substantial room for viable heavy neutral leptons.

We investigated three representative classes of electroweak scale seesaw models: Case-RS, SC, and SS. These cases span small, large, and ultraweak couplings of the electroweak right-handed neutrinos to the SM sector, while reproducing the observed light neutrino mass hierarchy and mixing pattern. We present a detailed calculation of the seesaw mixing using the two-component spinor formalism, which also serves as a, somehow missing in the existing literature, pedagogical review of the Type-I seesaw mechanism, provided in Appendix B. Building on this, all seesaw parameters in our analysis, including the couplings of the right-handed neutrinos to the SM, are obtained from a consistent seesaw framework using the PSO algorithm, rather than from rough order-of-magnitude estimates as in part of the existing literature. We then embedded these seesaw constructions into a minimal dark sector containing a fermion χ and a complex scalar ϕ , which communicate with the SM solely through renormalizable Yukawa interactions with the right-handed neutrinos.

We solved the full set of Boltzmann equations, including all relevant interactions involving light and heavy neutrinos after seesaw mixing, and thereby determined the complete evolution of the dark particles. We find that there is a wide region of viable parameter space reproducing the observed dark matter relic abundance, demonstrating that electroweak right-handed neutrino portal dark matter provides a robust framework in light of current and future searches. Among the three representative cases, Case-SC is particularly interesting, as the right-handed neutrinos couple to the SM sector with sizable couplings as large as $\mathcal{O}(10^{-2})$, making this scenario especially promising for collider searches and neutrino experiments.

For ultraweak seesaw couplings, we show that strong internal interactions within the dark sector can have a significant impact on freeze-in predictions. In Case-SS, where the portal right-handed neutrino never thermalizes with the SM, the dark sector can only be produced via freeze-in. When the hidden sector couplings are large enough to drive χ and ϕ toward internal equilibrium, the evolution of the dark sector can no longer be captured by treating each species as an independent freeze-in component. We explicitly compare the full multi-temperature evolution with a commonly used approximate treatment in which one computes the freeze-in production of χ , ϕ and right-handed neutrinos separately, neglecting their mutual interactions, and then allows the unstable particles to decay only after freeze-in. In representative benchmark models, we find that this simplified procedure underestimates the final dark matter abundance by about 30% when three-point internal interactions such

as $\mathbb{N} \leftrightarrow \chi\phi$ are present, or by more than 95% when such interactions are absent. This demonstrates that a careful treatment of dark sector dynamics is essential in right-handed neutrino portal freeze-in models.

Overall, our results show that electroweak scale right-handed neutrino portal dark matter provides a robust and predictive framework linking neutrino masses, the dark matter relic abundance, and the properties of heavy neutral leptons. The three seesaw realizations we examined offer qualitatively different patterns of portal couplings and thermal histories, yet all admit viable benchmark models in which the observed relic density is obtained in concordance with current laboratory and cosmological bounds. Because the same heavy Majorana fields govern both neutrino and dark sector phenomenology, this framework is highly testable: collider searches for heavy neutral leptons, precision probes of neutrino mixing and unitarity, and improved cosmological measurements will further constrain, or potentially reveal, the parameter space explored here.

Acknowledgments:

This work is supported in part by the National Natural Science Foundation of China under Grant No. 11935009, and Tianjin University Self-Innovation Fund Extreme Basic Research Project Grant No. 2025XJ21-0007.

A Notations and useful formulas

Convention on the charge conjugation We use the metric $\text{diag}\{+, - - -\}$. The charge conjugation operation is defined as

$$C : \psi \rightarrow \psi^c \quad \psi^c \equiv -i\gamma^2\psi^* = -i(\bar{\psi}\gamma^0\gamma^2)^T = -i\gamma^2\gamma^0\bar{\psi}^T. \quad (54)$$

The gamma matrices are given by

$$\gamma^\mu = \begin{pmatrix} 0 & \sigma^\mu \\ \bar{\sigma}^\mu & 0 \end{pmatrix}, \quad \sigma^\mu = (\mathbf{1}, \vec{\sigma}), \quad \bar{\sigma}^\mu = (\mathbf{1}, -\vec{\sigma}). \quad (55)$$

γ^0, γ^2 are symmetric matrices, each equal to its own transpose

$$\gamma^0 = \begin{pmatrix} 0 & \mathbf{1} \\ \mathbf{1} & 0 \end{pmatrix} = \begin{pmatrix} & 1 & \\ 1 & & \\ & & 1 \end{pmatrix}, \quad \gamma^2 = \begin{pmatrix} 0 & \sigma_2 \\ -\sigma_2 & 0 \end{pmatrix} = \begin{pmatrix} & & -i \\ & i & \\ -i & & \end{pmatrix}. \quad (56)$$

Thus a charge conjugation $C : \psi \rightarrow \psi^c$ transforms a Dirac field to be

$$C : \psi = \begin{pmatrix} \psi_L \\ \psi_R \end{pmatrix} \equiv \begin{pmatrix} \xi \\ \eta \end{pmatrix} \longrightarrow \psi^c = -i\gamma^2\psi^* = \begin{pmatrix} -i\sigma_2\psi_R^* \\ i\sigma_2\psi_L^* \end{pmatrix} = \begin{pmatrix} -i\sigma_2\eta^* \\ i\sigma_2\xi^* \end{pmatrix}. \quad (57)$$

A Majorana fermion ψ_M is defined as $\psi_M = \psi_M^c$ and thus a Majorana 4-spinor can be defined by either using a left-handed 2-component spinor ξ

$$\psi_M = \begin{pmatrix} \xi \\ \xi^c \end{pmatrix} = \begin{pmatrix} \xi \\ i\sigma_2\xi^* \end{pmatrix}, \quad (58)$$

or using a right-handed 2-component spinor η

$$\psi_M = \begin{pmatrix} \eta^c \\ \eta \end{pmatrix} = \begin{pmatrix} -i\sigma_2\eta^* \\ \eta \end{pmatrix}, \quad (59)$$

it's therefore convenient to define the charge conjugation for two-component spinor fields as the following

$$\text{for left-handed field } \xi : \quad \xi^c \equiv i\sigma_2\xi^*, \quad (60)$$

$$\text{for right-handed field } \eta : \quad \eta^c \equiv -i\sigma_2\eta^*. \quad (61)$$

Dirac and Majorana mass terms For the Dirac fermion

$$\psi = \begin{pmatrix} \psi_L \\ \psi_R \end{pmatrix} = \begin{pmatrix} \xi \\ \eta \end{pmatrix},$$

its Dirac mass term can be written in terms of two-component spinors

$$-\mathcal{L} = m_D\bar{\psi}\psi = m_D(\bar{\psi}_L\psi_R + \bar{\psi}_R\psi_L) = m_D(\xi^\dagger\eta + \eta^\dagger\xi). \quad (62)$$

The key step in the seesaw mechanism is to rewrite the Dirac mass terms in terms of charge conjugate fields, to mix with the Majorana mass terms

$$-\mathcal{L} = m_D\bar{\psi}\psi = m_D(\xi^{c\dagger}\eta^c + \eta^{c\dagger}\xi^c), \quad (63)$$

which can be verified by

$$\begin{aligned} \xi^{c\dagger}\eta^c &= (i\sigma_2\xi^*)^\dagger(-i\sigma_2\eta^*) = -\xi^T\eta^* \\ &= -\begin{pmatrix} \xi_1 & \xi_2 \end{pmatrix} \begin{pmatrix} \eta_1^* \\ \eta_2^* \end{pmatrix} = \begin{pmatrix} \eta_1^* & \eta_2^* \end{pmatrix} \begin{pmatrix} \xi_1 \\ \xi_2 \end{pmatrix} = \eta^\dagger\xi. \end{aligned} \quad (64)$$

On the other hand, a Majorana mass term is defined as

$$-\mathcal{L}_M = \frac{M}{2}\bar{\psi}_M\psi_M, \quad (65)$$

for the 4-component Majorana fermion

$$\psi_M = \begin{pmatrix} \psi_{M,L} \\ \psi_{M,R} \end{pmatrix} = \begin{pmatrix} \xi \\ \eta \end{pmatrix}, \quad \text{with } \eta = \xi^c. \quad (66)$$

The Majorana mass term can be written in terms of either the left-handed two-component spinor ξ

$$-\mathcal{L}_M^L = \frac{M}{2}(\xi^{c\dagger}\xi + \xi^\dagger\xi^c) = \frac{M}{2}[\xi^T(-i\sigma_2)\xi + \xi^\dagger(i\sigma_2)\xi^*], \quad (67)$$

or in terms of the right-handed two-component spinor η

$$-\mathcal{L}_M^R = \frac{M}{2}(\eta^{c\dagger}\eta + \eta^\dagger\eta^c) = \frac{M}{2}[\eta^T(i\sigma_2)\eta + \eta^\dagger(-i\sigma_2)\eta^*]. \quad (68)$$

Neutrino masses in the SM The SM contains only left-handed neutrinos and we have ($i = e, \mu, \tau$)

$$V_{\text{SM}i} = \begin{pmatrix} \nu_{iL} \\ 0 \end{pmatrix} \equiv \begin{pmatrix} \nu_i \\ 0 \end{pmatrix}, \quad 2 \text{ d.o.f.} \quad (69)$$

Mass terms can be generated by introducing gauge-singlet right-handed neutrinos

$$\begin{pmatrix} 0 \\ \nu_{iR} \end{pmatrix}, \quad (70)$$

and we define the right-handed neutrino in the full Majorana 4-spinor form

$$\mathbb{N}_i = \begin{pmatrix} -i\sigma_2\nu_{iR}^* \\ \nu_{iR} \end{pmatrix} \equiv \begin{pmatrix} -i\sigma_2 N_i^* \\ N_i \end{pmatrix}, \quad 2 \text{ d.o.f.}, \quad (71)$$

where we use N instead of ν_R to avoid future confusions. From this point forward, we will use normal capital letters to denote Dirac 4-spinors; and use capital letters with double lines, such as \mathbb{N} and \mathbb{V} , to denote Majorana 4-spinors.

We note that the use of the subscripts “ L ” and “ R ” to denote left-handed and right-handed fields can be confusing. For instance, “ ν_R ”, typically identified as the right-handed neutrino, may refer either to the right-handed component of a 4-spinor, which is 2-component, or to a right-handed Majorana 4-spinor. This ambiguity becomes particularly problematic when performing charge conjugation on spinors labeled with “ L ” and “ R ”. We thus define two-component spinors ν_i, N_i , representing the two-component left-handed SM neutrinos and right-handed Majorana neutrinos respectively. Thus in the flavor basis, the full neutrino Dirac 4-spinor reads

$$V_i = \begin{pmatrix} \nu_{iL} \\ \nu_{iR} \end{pmatrix} \equiv \begin{pmatrix} \nu_i \\ N_i \end{pmatrix}, \quad 4 \text{ d.o.f.} \quad (72)$$

B Seesaw mechanism for one generation, details

In this Appendix, we present the most detailed derivation of seesaw-induced neutrino mixing available in the literature, which is surprisingly rare. This derivation explicitly determines the couplings of all neutrinos (three light and three heavy) to SM particles Eqs. (10)–(13) and to dark sector particles Eq. (35) after the seesaw mixing. Such couplings are of significant importance in models where the dark sector communicates with the SM via Majorana neutrinos. In many related works, it is often assumed, almost by default, that the dark sector is effectively decoupled from the SM due to the smallness of the mixing angles. As a result, interactions between dark sector particles and SM fields (e.g., light neutrinos, gauge bosons and the Higgs boson), mediated by the Majorana neutrinos, are frequently neglected. This omission is common given the complexity of a complete analysis, but in some cases it can lead to errors.

The full mass term for a one-generation neutrino is written as

$$\mathcal{L}_{\text{mass}} = -y_{ij}^\nu \bar{L}_i \tilde{H} P_R \mathbb{N}_j - \frac{M_i}{2} \overline{\mathbb{N}_i} \mathbb{N}_i + h.c., \quad (73)$$

where $\tilde{H} = i\sigma_2 H$. In terms of 2-component spinors,

$$\begin{aligned}\mathcal{L}_{\text{mass}}^{\text{neutrino}} &= -\frac{y_{ij}^\nu v}{\sqrt{2}}(\nu_i^\dagger N_j + N_j^\dagger \nu_i) - \frac{M_i}{2}[N_i^T(i\sigma_2)N_i + (N_i^*)^T(-i\sigma_2)N_i^*] \\ &\rightarrow -\frac{m_D}{2}(\nu^\dagger N + N^\dagger \nu + N^{\text{c}\dagger} \nu^c + \nu^{\text{c}\dagger} N^c) - \frac{M_i}{2}(N^\dagger N^c + N^{\text{c}\dagger} N)\end{aligned}\quad (74)$$

where in the second line we derive the one-generation case for illustration and we define $m_D = y_{ij}^\nu v/\sqrt{2} \rightarrow y^\nu v/\sqrt{2}$ and

$$\nu^c \equiv +i\sigma_2 \nu^*, \quad N^c \equiv -i\sigma_2 N^*. \quad (75)$$

Hence we can obtain the mass mixing matrix:

$$\mathcal{L}_{\text{mass}}^{\text{neutrino}} = -\frac{1}{2} \begin{pmatrix} \nu^{\text{c}\dagger} & N^\dagger \end{pmatrix} \begin{pmatrix} 0 & m_D \\ m_D & M \end{pmatrix} \begin{pmatrix} \nu \\ N^c \end{pmatrix} - \frac{1}{2} \begin{pmatrix} \nu^\dagger & N^{\text{c}\dagger} \end{pmatrix} \begin{pmatrix} 0 & m_D \\ m_D & M \end{pmatrix} \begin{pmatrix} \nu^c \\ N \end{pmatrix}, \quad (76)$$

and these two terms are just the hermitian conjugate of each other. First we analyze the first term:

$$\begin{aligned}\text{1st term} &= -\frac{1}{2} \begin{pmatrix} \nu^{\text{c}\dagger} & N^\dagger \end{pmatrix} \begin{pmatrix} 0 & m_D \\ m_D & M \end{pmatrix} \begin{pmatrix} \nu \\ N^c \end{pmatrix} \\ &= -\frac{1}{2} \begin{pmatrix} (i\sigma_2 \nu^*)^\dagger & N^\dagger \end{pmatrix} O O^T \begin{pmatrix} 0 & m_D \\ m_D & M \end{pmatrix} O O^T \begin{pmatrix} \nu \\ -i\sigma_2 N^* \end{pmatrix} \\ &= -\frac{1}{2} \begin{pmatrix} \nu^T (-i\sigma_2) & (N^*)^T (i\sigma_2) (-i\sigma_2) \end{pmatrix} O O^T \begin{pmatrix} 0 & m_D \\ m_D & M \end{pmatrix} O O^T \begin{pmatrix} \nu \\ -i\sigma_2 N^* \end{pmatrix} \\ &= -\frac{1}{2} \begin{pmatrix} \nu^T & (-i\sigma_2 N^*)^T \end{pmatrix} (-i\sigma_2) O O^T \begin{pmatrix} 0 & m_D \\ m_D & M \end{pmatrix} O O^T \begin{pmatrix} \nu \\ -i\sigma_2 N^* \end{pmatrix} \\ &= -\frac{1}{2} \begin{pmatrix} \nu^T & (-i\sigma_2 N^*)^T \end{pmatrix} O (-i\sigma_2) O^T \begin{pmatrix} 0 & m_D \\ m_D & M \end{pmatrix} O O^T \begin{pmatrix} \nu \\ -i\sigma_2 N^* \end{pmatrix} \\ &= -\frac{1}{2} \begin{pmatrix} \nu_\ell^T & \nu_h^T \end{pmatrix} (-i\sigma_2) \begin{pmatrix} m_\ell & 0 \\ 0 & m_h \end{pmatrix} \begin{pmatrix} \nu_\ell \\ \nu_h \end{pmatrix} \\ &\Rightarrow -\frac{1}{2} \begin{pmatrix} \nu_\ell^{(L)T} & \nu_h^{(L)T} \end{pmatrix} (-i\sigma_2) \begin{pmatrix} m_\ell & 0 \\ 0 & m_h \end{pmatrix} \begin{pmatrix} \nu_\ell^{(L)} \\ \nu_h^{(L)} \end{pmatrix} \\ &= -\frac{1}{2} [m_\ell \nu_\ell^{(L)T} (-i\sigma_2) \nu_\ell^{(L)} + m_h \nu_h^{(L)T} (-i\sigma_2) \nu_h^{(L)}].\end{aligned}$$

The 2×2 orthogonal matrix O (in the full three-generation seesaw mixing case, the orthogonal matrix is 6×6), can pass through $(-i\sigma_2)$, since O operates only on the neutrino flavor basis, whereas $(-i\sigma_2)$ acts only on the two-component spinors, which can be seen schematically as

$$\begin{aligned}\mathbf{V}^T \mathbf{M} \mathbf{V} &= \mathbf{V}_{I,a}^T (-i\sigma_2)_{ab} \mathbf{M}_{IJ} \mathbf{V}_{J,b} = \mathbf{V}_{I,a}^T (-i\sigma_2)_{ab} O_{IP} (O^T \mathbf{M} O)_{PQ} O_{QJ}^T \mathbf{V}_{J,b} \\ &= \mathbf{V}_{I,a}^T O_{IP} (-i\sigma_2)_{ab} (O^T \mathbf{M} O)_{PQ} O_{QJ}^T \mathbf{V}_{J,b}.\end{aligned}\quad (77)$$

The mass eigenbasis is defined by

$$O^T \begin{pmatrix} \nu \\ -i\sigma_2 N^* \end{pmatrix} \equiv \begin{pmatrix} \nu_\ell \\ \nu_h \end{pmatrix}, \quad (78)$$

where the orthogonal matrix O is determined by diagonalizing the mass matrix. One can see from the last step that ν_ℓ and ν_h are indeed left-handed (component) Majorana fields, c.f., Eqs. (58) and (67). The derivation of the second term is similar

$$\begin{aligned} \text{2nd term} &= -\frac{1}{2} \begin{pmatrix} \nu^\dagger & N^{c\dagger} \end{pmatrix} \begin{pmatrix} 0 & m_D \\ m_D & M \end{pmatrix} \begin{pmatrix} \nu^c \\ N \end{pmatrix} \\ &= -\frac{1}{2} \begin{pmatrix} (\nu^*)^T & [(-i\sigma_2 N^*)^*]^T \end{pmatrix} \begin{pmatrix} 0 & m_D \\ m_D & M \end{pmatrix} \begin{pmatrix} i\sigma_2 \nu^* \\ N \end{pmatrix} \\ &= -\frac{1}{2} \begin{pmatrix} (i\sigma_2 \nu^*)^T & N^T \end{pmatrix} (i\sigma_2) O O^T \begin{pmatrix} 0 & m_D \\ m_D & M \end{pmatrix} O O^T \begin{pmatrix} i\sigma_2 \nu^* \\ N \end{pmatrix} \\ &= -\frac{1}{2} \begin{pmatrix} \nu_\ell^T & \nu_h^T \end{pmatrix} (i\sigma_2) \begin{pmatrix} m_\ell & 0 \\ 0 & m_h \end{pmatrix} \begin{pmatrix} \nu_\ell \\ \nu_h \end{pmatrix} \\ &\Rightarrow -\frac{1}{2} \begin{pmatrix} \nu_\ell^{(R)T} & \nu_h^{(R)T} \end{pmatrix} (i\sigma_2) \begin{pmatrix} m_\ell & 0 \\ 0 & m_h \end{pmatrix} \begin{pmatrix} \nu_\ell^{(R)} \\ \nu_h^{(R)} \end{pmatrix} \\ &= -\frac{1}{2} [m_\ell \nu_\ell^{(R)T} (i\sigma_2) \nu_\ell^{(R)} + m_h \nu_h^{(R)T} (i\sigma_2) \nu_h^{(R)}], \end{aligned}$$

which is the Majorana mass term for the right-handed fields.

The diagonalization of the mass matrix is identical for both the first and the second terms

$$O^T \begin{pmatrix} 0 & m_D \\ m_D & M \end{pmatrix} O \approx \begin{pmatrix} 1 & \frac{m_D}{M} \\ -\frac{m_D}{M} & 1 \end{pmatrix} \begin{pmatrix} 0 & m_D \\ m_D & M \end{pmatrix} \begin{pmatrix} 1 & -\frac{m_D}{M} \\ \frac{m_D}{M} & 1 \end{pmatrix} \approx \begin{pmatrix} m_\ell & 0 \\ 0 & m_h \end{pmatrix}, \quad (79)$$

for $m_D \ll M$, and the two mass eigenvalues are

$$m_h \approx M, \quad m_\ell \approx \frac{m_D^2}{M} = \frac{y^2 v^2}{2M}. \quad (80)$$

For the set of values $y^\nu \sim \mathcal{O}(1)$, $M \sim \text{GUT} \sim 10^{14-15}$ GeV (GUT Majorana right-handed neutrinos), or $y^\nu \sim 10^{-7} - 10^{-6}$, $M \sim 100 - 1000$ GeV (EW–TeV Majorana right-handed neutrinos), one roughly gets $m_\ell \sim 10^{-2}$ eV, which is about the correct order of the light neutrino masses.

Using the rotation matrix O we obtain the mass eigenbasis

$$\mathbb{V}_\ell = \begin{pmatrix} \nu_\ell^{(L)} \\ \nu_\ell^{(R)} \end{pmatrix} = \begin{pmatrix} \nu + \frac{m_D}{M} (-i\sigma_2 N^*) \\ i\sigma_2 \nu^* + \frac{m_D}{M} N \end{pmatrix}, \quad (81)$$

$$\mathbb{V}_h = \begin{pmatrix} \nu_h^{(L)} \\ \nu_h^{(R)} \end{pmatrix} = \begin{pmatrix} -\frac{m_D}{M} \nu - i\sigma_2 N^* \\ -\frac{m_D}{M} (i\sigma_2 \nu^*) + N \end{pmatrix}. \quad (82)$$

One easily verifies

$$\mathbb{V}_\ell^c = \mathbb{V}_\ell, \quad \mathbb{V}_h^c = \mathbb{V}_h, \quad (83)$$

and thus they are Majorana fields. Recall the right-handed majorana neutrino \mathbb{N} and further define a new Majorana field \mathbb{V} using the original SM left-handed neutrino ν :

$$\mathbb{V} \equiv \begin{pmatrix} \nu \\ i\sigma_2\nu^* \end{pmatrix}, \quad \mathbb{N} = \begin{pmatrix} -i\sigma_2 N^* \\ N \end{pmatrix}, \quad (84)$$

one writes down the final results:

$$\mathbb{V}_\ell = \mathbb{V} + \frac{m_D}{M}\mathbb{N}, \quad (85)$$

$$\mathbb{V}_h = -\frac{m_D}{M}\mathbb{V} + \mathbb{N}, \quad (86)$$

where $\mathbb{V}_\ell, \mathbb{V}_h$ are the mass eigenstates for the light and heavy Majorana neutrinos, and are constructed using the SM neutrino fields ν (only left-handed, 2 d.o.f.) and the seesaw right-handed Majorana neutrino N (also 2 d.o.f.). Especially, \mathbb{V}_ℓ is supposed to be the (observed) light neutrino.

On the other hand, one can express the original basis in terms of the mass eigenbasis

$$\mathbb{V} = \mathbb{V}_\ell - \frac{m_D}{M}\mathbb{V}_h, \quad (87)$$

$$\mathbb{N} = \frac{m_D}{M}\mathbb{V}_\ell + \mathbb{V}_h. \quad (88)$$

Hence, all SM interactions will be modified:

$$\begin{aligned} \mathcal{L}_{W^-} &\sim W_\mu^- \bar{e}_L \gamma^\mu \nu_L = W_\mu^- \bar{e}_L \gamma^\mu P_L V_{\text{SM}} = W_\mu^- \bar{e}_L \gamma^\mu P_L \mathbb{V} \\ &= W_\mu^- \bar{e}_L \gamma^\mu P_L \left(\mathbb{V}_\ell - \frac{m_D}{M} \mathbb{V}_h \right) \\ &\approx W_\mu^- \bar{e}_L \gamma^\mu P_L \mathbb{V}_\ell - \frac{m_D}{M} W_\mu^- \bar{e}_L \gamma^\mu P_L \mathbb{V}_h, \end{aligned} \quad (89)$$

$$\begin{aligned} \mathcal{L}_{W^+} &\sim W_\mu^+ \bar{\nu}_L \gamma^\mu e_L = W_\mu^+ \bar{V}_{\text{SM}} P_R \gamma^\mu e_L = W_\mu^+ \bar{\mathbb{V}} P_R \gamma^\mu e_L \\ &= W_\mu^+ \left(\bar{\mathbb{V}}_\ell - \frac{m_D}{M} \bar{\mathbb{V}}_h \right) P_R \gamma^\mu e_L \\ &\approx W_\mu^+ \bar{\mathbb{V}}_\ell P_R \gamma^\mu e_L - \frac{m_D}{M} W_\mu^+ \bar{\mathbb{V}}_h \gamma^\mu e_L. \end{aligned} \quad (90)$$

We can see clearly the charged current couplings for the SM (left-handed) neutrinos are not modified in the limit $m_D \ll M$, but now we also have the heavy neutrino couplings. The neutral current coupling is modified to be

$$\begin{aligned} \mathcal{L}_Z &\sim Z_\mu \bar{\nu}_L \gamma^\mu \nu_L = Z_\mu \bar{V}_{\text{SM}} P_R \gamma^\mu P_L V_{\text{SM}} = Z_\mu \bar{\mathbb{V}} P_R \gamma^\mu P_L \mathbb{V} \\ &= Z_\mu \left(\bar{\mathbb{V}}_\ell - \frac{m_D}{M} \bar{\mathbb{V}}_h \right) P_R \gamma^\mu P_L \left(\mathbb{V}_\ell - \frac{m_D}{M} \mathbb{V}_h \right) \\ &\approx Z_\mu \bar{\mathbb{V}}_\ell \gamma^\mu P_L \mathbb{V}_\ell - \frac{m_D}{M} Z_\mu \left(\bar{\mathbb{V}}_\ell \gamma^\mu P_L \mathbb{V}_h + \bar{\mathbb{V}}_h \gamma^\mu P_L \mathbb{V}_\ell \right). \end{aligned} \quad (91)$$

Finally the Higgs coupling:

$$\begin{aligned} \mathcal{L}_H &\sim h(\nu^\dagger N + N^\dagger \nu) = h(\bar{V}_{\text{SM}} \mathbb{N} + \bar{\mathbb{N}} V_{\text{SM}}) = h(\bar{\mathbb{V}} P_R \mathbb{N} + \bar{\mathbb{N}} P_L \mathbb{V}) \\ &= h \left(\bar{\mathbb{V}}_\ell - \frac{m_D}{M} \bar{\mathbb{V}}_h \right) P_R \left(\frac{m_D}{M} \mathbb{V}_\ell + \mathbb{V}_h \right) + h \left(\frac{m_D}{M} \bar{\mathbb{V}}_\ell + \bar{\mathbb{V}}_h \right) P_L \left(\mathbb{V}_\ell - \frac{m_D}{M} \mathbb{V}_h \right) \\ &\approx h(\bar{\mathbb{V}}_\ell P_R \mathbb{V}_h + \bar{\mathbb{V}}_h P_L \mathbb{V}_\ell) + \frac{m_D}{M} h(\bar{\mathbb{V}}_\ell \mathbb{V}_\ell - \bar{\mathbb{V}}_h \mathbb{V}_h). \end{aligned} \quad (92)$$

C PMNS parameterizations and the Dirac phase

The PDG parameterization of U_{PMNS} is

$$\begin{aligned}
 U_{\text{PMNS}}^{\text{PDG}} &= \begin{pmatrix} 1 & 0 & 0 \\ 0 & c_{23} & s_{23} \\ 0 & -s_{23} & c_{23} \end{pmatrix} \begin{pmatrix} c_{13} & 0 & s_{13}e^{-i\delta_{\text{CP}}} \\ 0 & 1 & 0 \\ -s_{13}e^{i\delta_{\text{CP}}} & 0 & c_{13} \end{pmatrix} \begin{pmatrix} c_{12} & s_{12} & 0 \\ -s_{12} & c_{12} & 0 \\ 0 & 0 & 1 \end{pmatrix} \begin{pmatrix} e^{i\eta_1} & 0 & 0 \\ 0 & e^{i\eta_2} & 0 \\ 0 & 0 & 1 \end{pmatrix} \\
 &= \begin{pmatrix} c_{12}c_{13} & s_{12}c_{13} & s_{13}e^{-i\delta_{\text{CP}}} \\ -s_{12}c_{23} - c_{12}s_{13}s_{23}e^{i\delta_{\text{CP}}} & c_{12}c_{23} - s_{12}s_{13}s_{23}e^{i\delta_{\text{CP}}} & c_{13}s_{23} \\ s_{12}s_{23} - c_{12}s_{13}c_{23}e^{i\delta_{\text{CP}}} & -c_{12}s_{23} - s_{12}s_{13}c_{23}e^{i\delta_{\text{CP}}} & c_{13}c_{23} \end{pmatrix} \begin{pmatrix} e^{i\eta_1} & 0 & 0 \\ 0 & e^{i\eta_2} & 0 \\ 0 & 0 & 1 \end{pmatrix}, \tag{93}
 \end{aligned}$$

where θ_{ij} are mixing angles and $s_{ij} \equiv \sin \theta_{ij}$, $c_{ij} \equiv \cos \theta_{ij}$; there is one Dirac phase δ_{CP} and two Majorana phases $\eta_{1,2}$.

The $\nu_\alpha \rightarrow \nu_\beta$ neutrino oscillation probability is given by theoretically:

$$P_{\alpha\beta} = \frac{\sum_i |U_{\alpha i}|^2 |U_{\beta i}|^2 + 2 \sum_{i < j} [\text{Re}(U_{\alpha i} U_{\beta j} U_{\alpha j}^* U_{\beta i}^*) \cos \Delta_{ij} - \text{Im}(U_{\alpha i} U_{\beta j} U_{\alpha j}^* U_{\beta i}^*) \sin \Delta_{ij}]}{(UU^\dagger)_{\alpha\alpha} (UU^\dagger)_{\beta\beta}}, \tag{94}$$

where $\Delta_{ij} = \frac{(m_i^2 - m_j^2)L}{2E}$, and E is beam energy. The probability $P_{\alpha\beta}$ is determined experimentally and depends on the ratio L/E . With various neutrino experiment data, and the measurements of $P_{ee}, P_{\mu\mu}, P_{\mu e}$, entries of the PMNS matrix can be determined.

Determine the seesaw parameters Type-I Seesaw mass matrix \mathbf{M} containing Dirac phases is a complex symmetric matrix can be diagnosed by Autonne-Takagi decomposition:

$$\mathbf{D} = U^T \mathbf{M} U = U^\dagger \mathbf{M}^\dagger U^*, \tag{95}$$

where \mathbf{D} is non-negative real diagonal matrix showing all mass eigenvalues, and U is a 6×6 unitary matrix, which transform the flavor basis into mass eigenbasis

$$U^\dagger \begin{pmatrix} \nu_e & \nu_\mu & \nu_\tau & N_1^c & N_2^c & N_3^c \end{pmatrix}^T = \begin{pmatrix} \mathbb{N}_1^{(L)} & \mathbb{N}_2^{(L)} & \dots & \dots & \mathbb{N}_6^{(L)} \end{pmatrix}^T. \tag{96}$$

ν_e, ν_μ, ν_τ are the left-handed SM neutrinos (two-component), $N_{1,2,3}$ are the right-handed Majorana neutrinos (two-component) introduced by the Seesaw Mechanism, and $\mathbb{N}_{1-6}^{(L)}$ are the left-handed components of Majorana fields, c.f., Eq. (58), in the mass eigenbasis.

Since the seesaw mixing is small, light neutrino mixing can be approximated using the upper-left 3×3 sub-matrix of U , denoted by $U_{3 \times 3}$

$$U_{3 \times 3}^\dagger \begin{pmatrix} \nu_e \\ \nu_\mu \\ \nu_\tau \end{pmatrix} \approx \begin{pmatrix} \mathbb{N}_1^{(L)} \\ \mathbb{N}_2^{(L)} \\ \mathbb{N}_3^{(L)} \end{pmatrix}, \quad U_{3 \times 3}^\dagger \begin{pmatrix} \nu_e^c \\ \nu_\mu^c \\ \nu_\tau^c \end{pmatrix} \approx \begin{pmatrix} \mathbb{N}_1^{(R)} \\ \mathbb{N}_2^{(R)} \\ \mathbb{N}_3^{(R)} \end{pmatrix}, \tag{97}$$

and thus $U_{3 \times 3}$ should match the PMNS matrix obtained from the neutrino experiment data.

Mixing angles θ_{ij} are determined by

$$\theta_{13} = \arcsin |U_{13}|, \quad \theta_{23} = \arctan \frac{|U_{23}|}{|U_{33}|}, \quad \theta_{12} = \arctan \frac{|U_{12}|}{|U_{11}|}, \quad (98)$$

and the Dirac phase can be calculated using the entries of $|U_{3 \times 3}|$, e.g.,

$$\delta_{\text{CP}} = \arccos \frac{|U_{21}|^2 - s_{12}^2 c_{23}^2 - c_{12}^2 s_{13}^2 s_{23}^2}{2s_{12}s_{23}s_{23}c_{12}c_{23}}, \quad (99)$$

which will be used to search for suitable seesaw benchmarks.

D Non-unitarity constraint

Light neutrino mixing matrix should be exactly unitary if the SM neutrinos have no mixing with the right-handed neutrinos, where the rotation matrix U takes a simplified form

$$\mathcal{U}_0 = \begin{pmatrix} U_0 & 0 \\ 0 & \mathbf{1}_{3 \times 3} \end{pmatrix}, \quad (100)$$

and thus the rotational matrix of SM neutrinos U_0 is unitary, which does not reflect the actual situation, since the PMNS matrix U_{PMNS} is not unitary. Allowing tiny mixing, the rotation matrix becomes

$$\mathcal{U} = \begin{pmatrix} U & U_1 \\ U_2 & U_N \end{pmatrix}, \quad (101)$$

which is still unitary while the top-left 3×3 block U should match the experimental fit of the (non-unitary) PMNS matrix U_{PMNS} . The top-right 3×3 block U_1 is related to U by

$$UU^\dagger + U_1 U_1^\dagger = \mathbf{1}_{3 \times 3}, \quad (102)$$

since the 6×6 rotation matrix \mathcal{U} is unitary. If the mixing is small such that all entries of the matrix U_1 are much less than 1, one has

$$\begin{aligned} UU^\dagger &\approx \mathbf{1}_{3 \times 3} - U_1 U_1^\dagger + \frac{1}{4} U_1 U_1^\dagger U_1 U_1^\dagger \\ &= \left(1 - \frac{1}{2} U_1 U_1^\dagger\right) \cdot \left(1 - \frac{1}{2} U_1 U_1^\dagger\right) \\ &= \left[\left(1 - \frac{1}{2} U_1 U_1^\dagger\right) U^0\right] \cdot \left[\left(1 - \frac{1}{2} U_1 U_1^\dagger\right) U^0\right]^\dagger, \end{aligned} \quad (103)$$

and thus the departure from unitarity of the matrix U can be approximately characterized by a 3×3 matrix $\eta \equiv \frac{1}{2} U_1 U_1^\dagger$ as

$$U = \left(1 - \frac{1}{2} U_1 U_1^\dagger\right) U_0 = (1 - \eta) U_0. \quad (104)$$

For the seesaw case

$$U_1 \approx \mathbf{M}_D \mathbf{M}_N^{-1}, \quad (105)$$

and thus η will be a real symmetric matrix if \mathbf{M}_D and \mathbf{M}_N are both real.

Conventional the matrix η is written as [64]

$$\eta = \begin{pmatrix} \eta_{ee} & \eta_{e\mu} & \eta_{e\tau} \\ \eta_{e\mu}^* & \eta_{\mu\mu} & \eta_{\mu\tau} \\ \eta_{e\tau}^* & \eta_{\mu\tau}^* & \eta_{\tau\tau} \end{pmatrix} \quad (106)$$

with diagonal elements real. Since U should match the experimental fit of the PMNS matrix, the entries of η matrix can be constrained by experimental data.

The $\nu_\alpha \rightarrow \nu_\beta$ neutrino oscillation probability, c.f., Eq. (94), can be further expressed by matrix entries of the η matrix in both short-baseline and long-baseline experiments. In this way, each entry of the η matrix will be constrained, imposing a further limitation on the mixing between the SM neutrinos and the right-handed neutrinos in the seesaw framework, which is referred to as the non-unitarity constraint.

Short-baseline experiments NOMAD [65] and NuTeV [66] have similar sensitivities to the zero-distance appearance probability, providing $P_{\mu e}^{\text{eff,SBL}} < 6 \times 10^{-4}$ at 90% C.L., while the combined bound is $P_{\mu e}^{\text{eff,SBL}} < 4 \times 10^{-4} (6 \times 10^{-4})$ at 90% (99%) C.L. according to [67]. Also in [67], long-baseline data coming from far detectors of T2K [68] and NOvA [69] are inferred from the measured spectra at their near detectors, so the effective appearance and disappearance oscillation probabilities relevant for these experiments need to be corrected because of the zero distance effects. In the analysis of MINOS/MINOS+ [70] data, neutral current (NC) events are considered in addition to charged current (CC) events. The NC sample is sensitive to the sum of the muon neutrino survival probability, the electron and tau neutrino appearance probabilities. Constraints from the combination of long-baseline and short-baseline experiments were derived in [64], and are reformulated as a restriction on η matrix entries as follows

Parameter	η_{ee}	$\eta_{\mu\mu}$	$\eta_{\tau\tau}$	$\eta_{e\mu}$	$\eta_{e\tau}$	$\eta_{\mu\tau}$
90% C.L.	0.031	0.005	0.110	0.0065	0.0165	0.0045
99% C.L.	0.056	0.010	0.220	0.0115	0.0325	0.0085

Table 3: Upper bounds of the non-unitarity parameters

E Scattering processes involving Majorana fermions

Three-point scattering Considering a Majorana fermion λ coupling to a complex scalar field ϕ and a Dirac fermion χ with the coupling constant g

$$\mathcal{L} = g\phi\bar{\psi}\lambda + g^*\phi^\dagger\bar{\lambda}\psi. \quad (107)$$

Consider the case: $m_\lambda > m_\psi + m_\phi$. In this case the Majorana fermion λ can decay to $\psi + \bar{\phi}$ and their anti-particle pair. First consider the decaying processes $\lambda(q) \rightarrow \psi(p) + \bar{\phi}(k)$ with $q = p + k$. The wick contraction is given by

$$\langle \text{out} | \overbrace{g\phi\bar{\psi}\lambda} \text{in} \rangle = g\bar{u}(p)u_M(q), \quad (108)$$

where the lower subscript M indicates the Majorana wave function. Following the regular Feynman rule, the $\lambda|\text{in}\rangle$ contraction corresponding to an incoming particle. The same process can be also interpreted as an incoming antifermion with momentum $-p$ combining with an incoming ϕ with momentum $-k$, producing an “antifermion” with momentum $-q$, and the corresponding amplitude is written as

$$\langle \text{out} | g \phi \bar{\psi} \lambda | \text{in} \rangle = -g \bar{v}(-p) v_M(-q), \quad (109)$$

with λ outgoing with a momentum $-q$ and ψ incoming with a momentum $-p$, and thus ϕ is also incoming with momentum $-k$. Here the $\bar{\psi}|\text{in}\rangle$ contraction gives rise to an incoming antifermion with momentum $-p$ and $\langle \text{out} | \lambda$ corresponds to an outgoing antifermion with momentum $-q$. The extra minus sign is coming from taking the $\langle \text{out} | \lambda$ contraction by exchange the order of the two fermionic fields ψ and λ .

As the spinor product should come out to be a value,

$$\begin{aligned} \bar{v}(-p) v_M(-q) &= [\bar{v}(-p) v_M(-q)]^T = [v^\dagger(-p) \gamma^0 v_M(-q)]^T = v_M^T(-q) (\gamma^0)^T v^{\dagger T}(-p) \\ &= v_M^T(-q) \bar{v}^T(-p) = v_M^T(-q) C^T C \bar{v}^T(-p) = \bar{u}_M^s(-q) C^T C^T u(-p) \\ &= -\bar{u}_M(-q) u(-p). \end{aligned} \quad (110)$$

where we have used $C \equiv -i\gamma^2\gamma^0$ and

$$C^T C = +1, \quad C^T C^T = -1. \quad (111)$$

The charge conjugation of the positive / negative energy wave functions are

$$u = -i\gamma^2 v^* = -i\gamma^2 \gamma^0 \bar{v}^T = C \bar{v}^T, \quad (112)$$

$$u^T = \left[-i\gamma^2 \gamma^0 \bar{v}^T \right]^T = \bar{v} C^T, \quad (113)$$

$$v = -i\gamma^2 u^* = -i\gamma^2 \gamma^0 \bar{u}^T = C \bar{u}^T, \quad (114)$$

$$v^T = \left[-i\gamma^2 \gamma^0 \bar{u}^T \right]^T = \bar{u} C^T. \quad (115)$$

Thus we find

$$\langle \text{out} | g \phi \bar{\psi} \lambda | \text{in} \rangle = -g \bar{v}(-p) v_M(-q) = g \bar{u}_M(-q) u(-p). \quad (116)$$

The spin-sum gives rise to the same result:

$$g^2 \text{Tr}[(\not{p} + m_\psi)(\not{q} + m_\lambda)] = g^2 \text{Tr}[(-\not{p} + m_\psi)(-\not{q} + m_\lambda)] = g^2 \text{Tr}(\not{p}\not{q} + m_\psi m_\lambda). \quad (117)$$

On the other hand, the *h.c.* term contributes

$$\langle \text{out} | g^* \phi^\dagger \bar{\lambda} \psi | \text{in} \rangle = -g^* \bar{v}_M(p) v(p). \quad (118)$$

Four-point scattering To compute the quantum number (fermion number)-violating process such as $LL \rightarrow HH$ or $NN \rightarrow HH$ (Majorana fermion can be the external leg, or the propagator), the common approach is:

1. Choose an fermion-flow direction on each fermion line: for a Dirac fermion, the fermion-flow aligns with charge flow; whereas for a Majorana fermion, the fermion-flow direction is just a convention. Starting from an external fermion line, draw the fermion-flow arrow, passing through the propagator, and keep drawing until it goes out from another external leg.
2. For an external leg, compare its physical momentum direction and the fermion-flow direction just drawn. For an incoming fermion (antifermion) with its momentum direction opposite to the fermion-flow direction, the corresponding Feynman rule is \bar{v} (u) instead of u (\bar{v}). Similarly, for an outgoing fermion (antifermion) with its momentum direction opposite to the fermion-flow direction, the corresponding Feynman rule is v (\bar{u}) instead of \bar{u} (v).
3. Write down the spinor chain in the amplitude and compute the amplitude-square using usual techniques.

This fermion-flow formulation also applies to the above three-point scattering computations.

F RIS subtraction

In a Boltzmann system containing processes $AB \leftrightarrow G \leftrightarrow CD$, where G mediates the s -channel exchange $AB \leftrightarrow CD$, the contribution from real intermediate states (RIS) must be subtracted from the $2 \rightarrow 2$ cross-section, since the on-shell resonance at $s = M_G^2$ is already accounted for by the $1 \leftrightarrow 2$ processes $AB \leftrightarrow G$ and $G \leftrightarrow CD$. Such subtraction was discussed in [71, 72].

In the narrow-width limit $\Gamma_G \rightarrow 0$, the Breit-Wigner resonance approaches a Dirac delta function

$$\frac{1}{\pi} \frac{M_G \Gamma_G}{(s - M_G^2)^2 - M_G^2 \Gamma_G^2} \xrightarrow{\Gamma_G \rightarrow 0} \delta(s - M_G^2), \quad (119)$$

which can be seen from

$$\lim_{\Gamma_G \rightarrow 0} \int_{-\infty}^{\infty} \left[\frac{1}{\pi} \frac{M_G \Gamma_G}{(s - M_G^2)^2 - M_G^2 \Gamma_G^2} \right] ds = 1, \quad (120)$$

and for $s \neq M_G^2$

$$\lim_{\Gamma_G \rightarrow 0} \left[\frac{1}{\pi} \frac{M_G \Gamma_G}{(s - M_G^2)^2 - M_G^2 \Gamma_G^2} \right] = 0. \quad (121)$$

The Breit-Wigner contribution is negligible away from the resonance $s \neq m_G^2$. This approximation applies in the narrow-width regime $\Gamma_G \ll m_G$.

To compute the RIS-subtracted contribution $|\mathcal{M}^{\text{RIS}}|^2$, we rewrite the squared amplitude for $AB \leftrightarrow CD$ as

$$|\mathcal{M}|^2 \equiv D_F M = \frac{1}{[(s - m_G^2)^2 + m_G^2 \Gamma_G^2]} M$$

$$\xrightarrow{\Gamma_G \ll M_G} \frac{\pi}{m_G \Gamma_G} \delta(s - M_G^2) M \equiv D_{\text{elta}} M \quad (122)$$

$$\xrightarrow{\Gamma_G \ll M_G} \frac{\pi}{m_Q \Gamma_Q} \frac{2\epsilon^3/\pi}{[(s - m_Q^2)^2 + \epsilon^2]^2} M \equiv D_{\text{RIS}} M. \quad (123)$$

where M is the numerator of the amplitude square. In the third line we express the Dirac function using another analytic form for s away from M_G^2 and $\epsilon \equiv \Gamma_G/M_G$. The RIS-subtracted amplitude square for the process $AB \leftrightarrow CD$ can thus be computed in either of the following ways:

$$|\mathcal{M}^{\text{RIS-}}|^2 = |\mathcal{M}|^2 - |\mathcal{M}^{\text{RIS}}|^2 = (D_F - D_{\text{elta}})M, \quad (124)$$

$$\text{or} = (D_F - D_{\text{RIS}})M, \quad (125)$$

which is valid for s away from M_G^2 and removes the resonant contribution. The thermally averaged cross-section is then computed using the RIS-subtracted squared amplitude $|\mathcal{M}^{\text{RIS-}}|^2$.

Here are two remarks on the RIS subtraction:

- RIS subtraction is required only for s -channel processes.
- For $AB \leftrightarrow CD$ with multiple intermediate states G_i ($i > 1$), the interference terms in the squared amplitude do not lead to double counting; hence RIS subtraction is not needed.

G Relevant Feynman diagrams

Relevant Feynman diagrams involving the dark sector particles χ, ϕ and the light/heavy neutrinos $\mathbb{V}_{i=1-6}$ are summarized in Figs. 9, 10, 11.

H Multi-temperature universe and evolution of hidden sector particles

In this Appendix we review the derivation of the evolution of hidden sector particles and the hidden sector temperature [33], for the one hidden sector extension of the SM. Assuming the hidden sector interacts with the visible sector feebly and hidden sector possess a separate temperature T_h compared to the visible sector temperature T (the temperature of the observed universe). From Friedmann equations we have

$$\frac{d\rho_h}{dt} + 3H(\rho_h + p_h) = j_h, \quad (126)$$

where $\rho_h(p_h)$ is the hidden sector energy density (pressure) determined by all of the particles inside the hidden sector.

The total energy density in the universe ρ is a sum of ρ_h and ρ_v (the energy density in the visible sector), giving rise to the Hubble parameter depending on both T and T_h

$$H^2 = \frac{8\pi G_N}{3} [\rho_v(T) + \rho_h(T_h)] = \frac{8\pi G_N}{3} \left(\frac{\pi^2}{30} g_{\text{eff}}^v T^4 + \frac{\pi^2}{30} g_{\text{eff}}^h T_h^4 \right), \quad (127)$$

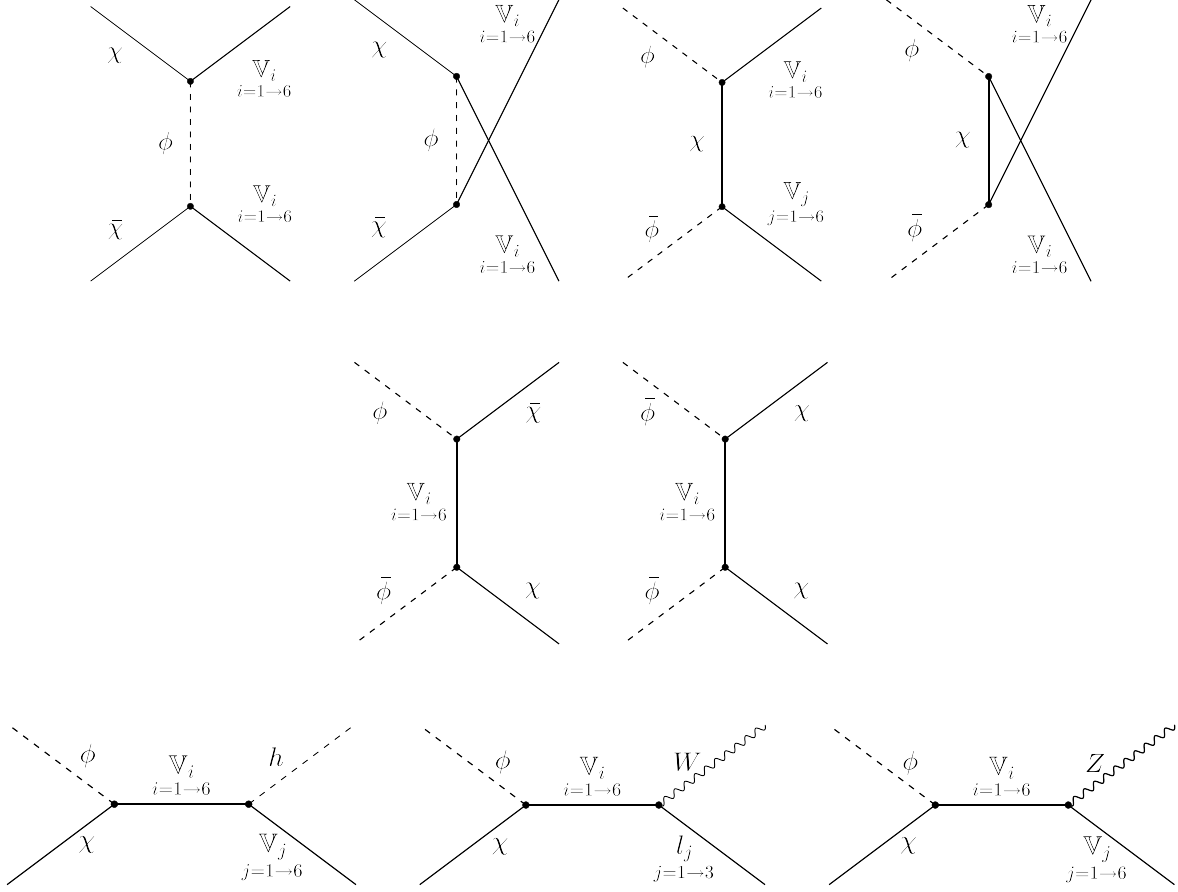


Figure 9: Relevant Feynman diagrams for $2 \rightarrow 2$ scattering processes are shown. The first row depicts dark particle χ, ϕ annihilation into light or heavy neutrinos after seesaw mixing; the inverse processes lead to freeze-in production of the dark sector particles. The second row shows internal dark sector interactions mediated by light or heavy neutrinos. The third row illustrates processes arising from $\chi\phi \rightarrow LH$ after electroweak symmetry breaking.

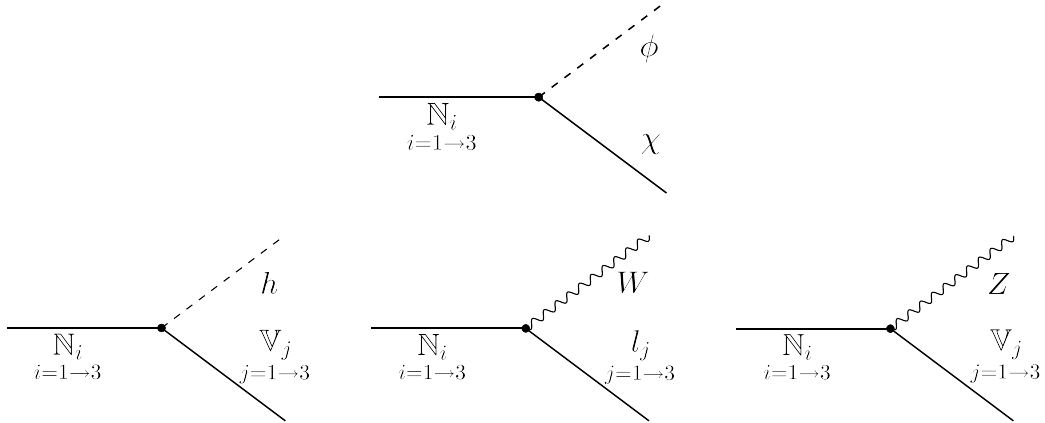


Figure 10: Feynman diagrams of the heavy neutrino $N_{1,2,3}$ decaying to dark sector particles χ, ϕ , and to SM particles.

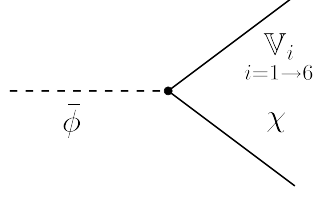


Figure 11: Feynman diagram of ϕ decay to χ and light (always present) or heavy (if $m_\phi > m_\chi + m_{N_i}$) neutrinos.

where g_{eff}^v (g_{eff}^h) is the visible (hidden) effective degrees of freedom. Further one can deduct the derivative of ρ_v, ρ_h w.r.t. T_h

$$\rho \frac{d\rho_h}{dT_h} = \left(\frac{\zeta_h}{\zeta} \rho_h - \frac{j_h}{4H\zeta} \right) \frac{d\rho}{dT_h}, \quad (128)$$

$$\frac{d\rho_v}{dT_h} = \frac{\zeta\rho_v + \rho_h(\zeta - \zeta_h) + j_h/(4H)}{\zeta_h\rho_h - j_h/(4H)} \frac{d\rho_h}{dT_h}, \quad (129)$$

where $\zeta = \frac{3}{4}(1 + p/\rho)$. Here $\zeta = 1$ is for the radiation dominated era and $\zeta = 3/4$ for the matter dominated universe. The total entropy of the universe is conserved and thus

$$s = \frac{2\pi^2}{45} (h_{\text{eff}}^v T^3 + h_{\text{eff}}^h T_h^3), \quad (130)$$

where h_{eff}^v (h_{eff}^h) is the visible (hidden) effective entropy degrees of freedom.

With manipulations of the above equations, the evolution of the ratio of temperatures for the two sectors $\eta(T_h) = T/T_h$ can be derived as

$$\frac{d\eta}{dT_h} = -\frac{A_v}{B_v} + \frac{\zeta\rho_v + \rho_h(\zeta - \zeta_h) + j_h/(4H)}{B_v[\zeta_h\rho_h - j_h/(4H)]} \frac{d\rho_h}{dT_h}, \quad (131)$$

with

$$A_v = \frac{\pi^2}{30} \left(\frac{dg_{\text{eff}}^v}{dT} \eta^5 T_h^4 + 4g_{\text{eff}}^v \eta^4 T_h^3 \right), \quad B_v = \frac{\pi^2}{30} \left(\frac{dg_{\text{eff}}^v}{dT} \eta^4 T_h^5 + 4g_{\text{eff}}^v \eta^3 T_h^4 \right). \quad (132)$$

The complete evolution of hidden sector particles can be obtained by solving the combined differential equations of the evolution equation for $\eta(T_h)$, together with the modified (temperature dependent) Boltzmann equations for the hidden sector particles, given by

$$\frac{dY_i}{dT_h} = -\frac{s}{H} \frac{d\rho_h/dT_h}{4\rho_h - j_h/H} \sum \left(-Y_i^2 \langle \sigma v \rangle_{\bar{i}i \rightarrow \times \times}^{T_h} + \dots \right), \quad (133)$$

where Y_i is the comoving number density of the i th hidden sector particle and the sum is over various scatter or decay processes involving this particle, which may depend on T_h (as shown by the example $\bar{i}i \rightarrow \times \times$) or depend on the visible sector T . The plus (minus) sign corresponds to increasing (decreasing) one number of the i th particle.

The complete Boltzmann equations for hidden sector particles as well as hidden sector temperatures for the freeze-in case are given in Section 4.2.

I Seesaw benchmark models

Benchmark-RS The regular seesaw benchmark parameters with electroweak right-handed neutrinos, c.f., Eq. (27), are given by 9 Yukawa couplings y_{ij}^ν in Eq. (14)

	\mathbb{N}_1^0	\mathbb{N}_2^0	\mathbb{N}_3^0
ν_e	1.00×10^{-7}	1.50×10^{-7}	2.11×10^{-8}
ν_μ	2.78×10^{-7}	1.00×10^{-7}	3.87×10^{-8}
ν_τ	$< 10^{-10}$	2.17×10^{-7}	4.60×10^{-7}

and three Majorana neutrino masses $M_1 = 200$ GeV, $M_2 = 220$ GeV, $M_3 = 260$ GeV, giving rise to the following seesaw mixing

	\mathbb{V}_1	\mathbb{V}_2	\mathbb{V}_3	\mathbb{N}_1	\mathbb{N}_2	\mathbb{N}_3
\mathbb{V}_1^0	0.82	0.56	0.14	8.70×10^{-8}	1.18×10^{-7}	1.41×10^{-8}
\mathbb{V}_2^0	0.46	0.47	0.75	2.41×10^{-7}	7.91×10^{-8}	2.59×10^{-7}
\mathbb{V}_3^0	0.36	0.68	0.64	1.17×10^{-19}	1.72×10^{-8}	3.07×10^{-7}
\mathbb{N}_1^0	3.96×10^{-8}	1.63×10^{-7}	1.95×10^{-7}	1.00	2.94×10^{-13}	2.13×10^{-13}
\mathbb{N}_2^0	6.63×10^{-8}	9.21×10^{-8}	8.76×10^{-8}	3.23×10^{-13}	1.00	1.51×10^{-13}
\mathbb{N}_3^0	2.59×10^{-9}	7.90×10^{-8}	3.94×10^{-7}	2.76×10^{-13}	1.78×10^{-13}	1.00

Benchmark-SC The structure cancellation with electroweak right-handed neutrinos has in total 17 parameters, c.f., Eq. (28), with three Majorana masses 200, 242, 282 GeV, two Yukawa couplings $Y_1 = 0.01$, $Y_2 = 0.0386$, two parameters $\alpha = 1.038392$, $\beta = 2.444289$, a fine-tuned small parameter $\epsilon = 6.34546 \times 10^{-10}$, and a 3×3 matrix X

-0.028039	-0.073682	-0.046258
0.1520252	0.3092630	-0.164200
0.1417292	0.2725134	0.0427021

giving rise to the following fine-tuned Yukawa couplings

	\mathbb{N}_1^0	\mathbb{N}_2^0	\mathbb{N}_3^0
ν_e	1.00×10^{-2}	3.86×10^{-2}	4.33×10^{-2}
ν_μ	1.04×10^{-2}	4.01×10^{-2}	4.50×10^{-2}
ν_τ	2.44×10^{-2}	9.44×10^{-2}	1.06×10^{-1}

and the final seesaw mixings for Case-SC are given by

	\mathbb{V}_1	\mathbb{V}_2	\mathbb{V}_3	\mathbb{N}_1	\mathbb{N}_2	\mathbb{N}_3
\mathbb{V}_1^0	0.83	-0.54	0.15	8.30×10^{-3}	2.79×10^{-2}	-2.68×10^{-2}
\mathbb{V}_2^0	0.31	0.67	0.67	8.70×10^{-3}	2.90×10^{-2}	-2.78×10^{-2}
\mathbb{V}_3^0	-0.47	-0.51	0.72	2.04×10^{-2}	6.82×10^{-2}	-6.54×10^{-2}
\mathbb{N}_1^0	5.18×10^{-14}	9.50×10^{-3}	-2.26×10^{-2}	1.00	9.40×10^{-3}	7.78×10^{-4}
\mathbb{N}_2^0	-2.09×10^{-14}	3.04×10^{-2}	-7.28×10^{-2}	-1.13×10^{-2}	9.97×10^{-1}	2.80×10^{-3}
\mathbb{N}_3^0	6.68×10^{-15}	-2.93×10^{-2}	7.01×10^{-2}	1.10×10^{-3}	3.20×10^{-3}	9.97×10^{-1}

Benchmark-SS For Case-SS, two of the right-handed neutrinos are responsible for generating the light-neutrino masses and mixings via the seesaw mechanism, while the third (assumed to be \mathbb{N}_1) couples only minimally to the SM. Consequently, the \mathbb{N}_1 portal to the dark sector can only generate the freeze-in production of dark particles.

We take three benchmark models for the Case-SS analysis, with different magnitudes of the y_1^ν coupling constant. Both models have 12 input parameters (9 Yukawa couplings and 3 Majorana masses).

Benchmark-SS1: The three Majorana masses are 360, 400, 507 GeV and 9 Yukawa couplings are given by

	\mathbb{N}_1^0	\mathbb{N}_2^0	\mathbb{N}_3^0
ν_e	5.000×10^{-11}	3.418×10^{-8}	2.255×10^{-7}
ν_μ	6.000×10^{-11}	6.552×10^{-7}	4.201×10^{-9}
ν_τ	7.000×10^{-11}	5.456×10^{-7}	3.826×10^{-7}

resulting in the seesaw mixing

	\mathbb{V}_1	\mathbb{V}_2	\mathbb{V}_3	\mathbb{V}_4	\mathbb{V}_5	\mathbb{V}_6
\mathbb{V}_1^0	0.8034	-0.5779	0.1430	2.416×10^{-11}	9.807×10^{-8}	1.173×10^{-8}
\mathbb{V}_2^0	0.3557	0.6586	0.6631	2.899×10^{-11}	1.827×10^{-9}	2.248×10^{-7}
\mathbb{V}_3^0	-0.4774	-0.4819	0.7347	3.823×10^{-11}	1.664×10^{-7}	1.872×10^{-7}
\mathbb{V}_4^0	-1.358×10^{-11}	1.117×10^{-11}	-4.753×10^{-11}	1.000	7.245×10^{-17}	3.218×10^{-17}
\mathbb{V}_5^0	1.027×10^{-15}	-5.105×10^{-8}	-2.883×10^{-7}	-4.531×10^{-17}	-1.551×10^{-13}	1.000
\mathbb{V}_6^0	1.496×10^{-15}	1.357×10^{-7}	-1.375×10^{-7}	-8.050×10^{-17}	1.000	1.224×10^{-13}

Benchmark-SS2: The three Majorana masses are again taken 360, 400, 507 GeV. Yukawa couplings and the resulting seesaw mixing are given by

	\mathbb{N}_1^0	\mathbb{N}_2^0	\mathbb{N}_3^0
ν_e	4.000×10^{-13}	2.255×10^{-7}	3.418×10^{-8}
ν_μ	6.000×10^{-13}	4.201×10^{-9}	6.522×10^{-7}
ν_τ	8.000×10^{-13}	3.826×10^{-7}	5.456×10^{-7}

	\mathbb{V}_1	\mathbb{V}_2	\mathbb{V}_3	\mathbb{V}_4	\mathbb{V}_5	\mathbb{V}_6
\mathbb{V}_1^0	0.8034	-0.5779	0.1430	1.933×10^{-13}	9.807×10^{-8}	1.1728×10^{-8}
\mathbb{V}_2^0	0.3557	0.6586	0.6631	2.899×10^{-13}	1.827×10^{-9}	2.248×10^{-7}
\mathbb{V}_3^0	-0.4774	-0.4819	0.7347	3.866×10^{-13}	1.664×10^{-7}	1.872×10^{-7}
\mathbb{V}_4^0	-7.386×10^{-14}	1.071×10^{-13}	-5.039×10^{-13}	1.000	7.543×10^{-19}	3.425×10^{-19}
\mathbb{V}_5^0	8.154×10^{-20}	1.357×10^{-7}	-1.375×10^{-7}	-8.381×10^{-19}	1.000	1.224×10^{-13}
\mathbb{V}_6^0	6.099×10^{-20}	-5.105×10^{-8}	-2.883×10^{-7}	-4.823×10^{-19}	-1.551×10^{-13}	1.000

Benchmark-SS3: The three Majorana masses are taken 225, 400, 507 GeV and 9 Yukawa couplings are given by

	N_1^0	N_2^0	N_3^0
ν_e	1.000×10^{-10}	3.418×10^{-8}	2.255×10^{-7}
ν_μ	2.000×10^{-10}	6.552×10^{-7}	4.201×10^{-9}
ν_τ	3.000×10^{-10}	5.456×10^{-7}	3.826×10^{-7}

This gives rise to the following seesaw mixing

	\mathbb{V}_1	\mathbb{V}_2	\mathbb{V}_3	\mathbb{V}_4	\mathbb{V}_5	\mathbb{V}_6
\mathbb{V}_1^0	0.8035	-0.5779	0.1430	7.731×10^{-11}	9.807×10^{-8}	1.173×10^{-8}
\mathbb{V}_2^0	0.3557	0.6586	0.6631	1.546×10^{-10}	1.827×10^{-9}	2.248×10^{-7}
\mathbb{V}_3^0	-0.4774	-0.4819	0.7347	2.319×10^{-10}	1.664×10^{-7}	1.872×10^{-7}
\mathbb{V}_4^0	-6.384×10^{-12}	5.462×10^{-11}	-2.840×10^{-10}	1.000	5.973×10^{-17}	6.312×10^{-17}
\mathbb{V}_5^0	1.905×10^{-15}	-5.105×10^{-8}	-2.883×10^{-7}	-1.422×10^{-16}	-1.551×10^{-13}	1.000
\mathbb{V}_6^0	2.355×10^{-15}	1.357×10^{-7}	-1.375×10^{-7}	-1.062×10^{-16}	1.000	1.224×10^{-13}

References

- [1] V. Khachatryan *et al.* [CMS], Phys. Lett. B **748**, 144-166 (2015) doi:10.1016/j.physletb.2015.06.070 [arXiv:1501.05566 [hep-ex]].
- [2] A. M. Sirunyan *et al.* [CMS], Phys. Rev. Lett. **120**, no.22, 221801 (2018) doi:10.1103/PhysRevLett.120.221801 [arXiv:1802.02965 [hep-ex]].
- [3] A. M. Sirunyan *et al.* [CMS], JHEP **01**, 122 (2019) doi:10.1007/JHEP01(2019)122 [arXiv:1806.10905 [hep-ex]].
- [4] A. Tumasyan *et al.* [CMS], Phys. Rev. Lett. **131**, no.1, 011803 (2023) doi:10.1103/PhysRevLett.131.011803 [arXiv:2206.08956 [hep-ex]].
- [5] G. Aad *et al.* [ATLAS], Eur. Phys. J. C **83**, no.9, 824 (2023) doi:10.1140/epjc/s10052-023-11915-y [arXiv:2305.14931 [hep-ex]].
- [6] A. Hayrapetyan *et al.* [CMS], JHEP **06**, 123 (2024) doi:10.1007/JHEP06(2024)123 [arXiv:2403.00100 [hep-ex]].
- [7] G. Aad *et al.* [ATLAS], Phys. Lett. B **856**, 138865 (2024) doi:10.1016/j.physletb.2024.138865 [arXiv:2403.15016 [hep-ex]].
- [8] T. Kozynets, P. Eller, A. Zander, M. Ettlgruber and D. J. Koskinen, JHEP **05**, 130 (2025) doi:10.1007/JHEP05(2025)130 [arXiv:2407.20388 [hep-ph]].
- [9] A. D. Dolgov, S. H. Hansen, G. Raffelt and D. V. Semikoz, Nucl. Phys. B **590**, 562-574 (2000) doi:10.1016/S0550-3213(00)00566-6 [arXiv:hep-ph/0008138 [hep-ph]].
- [10] I. A. Zelko, T. Treu, K. N. Abazajian, D. Gilman, A. J. Benson, S. Birrer, A. M. Nierenberg and A. Kusenko, Phys. Rev. Lett. **129**, no.19, 191301 (2022) doi:10.1103/PhysRevLett.129.191301 [arXiv:2205.09777 [hep-ph]].
- [11] B. M. Roach, S. Rossland, K. C. Y. Ng, K. Perez, J. F. Beacom, B. W. Grefenstette, S. Horiuchi, R. Krivonos and D. R. Wik, Phys. Rev. D **107**, no.2, 023009 (2023) doi:10.1103/PhysRevD.107.023009 [arXiv:2207.04572 [astro-ph.HE]].
- [12] G. H. Du, T. N. Li, P. J. Wu, L. Feng, S. H. Zhou, J. F. Zhang and X. Zhang, [arXiv:2501.10785 [astro-ph.CO]].
- [13] E. Cortina Gil *et al.* [NA62], Phys. Lett. B **807**, 135599 (2020) doi:10.1016/j.physletb.2020.135599 [arXiv:2005.09575 [hep-ex]].
- [14] E. Cortina Gil *et al.* [NA62], Phys. Lett. B **816**, 136259 (2021) doi:10.1016/j.physletb.2021.136259 [arXiv:2101.12304 [hep-ex]].
- [15] B. Bloch-Devaux *et al.* [NA62], [arXiv:2507.07345 [hep-ex]].
- [16] L. Köllenberger [KATRIN], PoS **DISCRETE2022**, 078 (2024) doi:10.22323/1.431.0078

- [17] H. Acharya *et al.* [KATRIN], *Nature* **648**, no.8092, 70-75 (2025) doi:10.1038/s41586-025-09739-9 [arXiv:2503.18667 [hep-ex]].
- [18] S. P. Li and X. J. Xu, *JCAP* **06**, 047 (2023) doi:10.1088/1475-7516/2023/06/047 [arXiv:2212.09109 [hep-ph]].
- [19] M. Escudero, N. Rius and V. Sanz, *JHEP* **02**, 045 (2017) doi:10.1007/JHEP02(2017)045 [arXiv:1606.01258 [hep-ph]].
- [20] M. Escudero, N. Rius and V. Sanz, *Eur. Phys. J. C* **77**, no.6, 397 (2017) doi:10.1140/epjc/s10052-017-4963-x [arXiv:1607.02373 [hep-ph]].
- [21] Y. L. Tang and S. h. Zhu, *JHEP* **01**, 025 (2017) doi:10.1007/JHEP01(2017)025 [arXiv:1609.07841 [hep-ph]].
- [22] P. Bandyopadhyay, E. J. Chun, R. Mandal and F. S. Queiroz, *Phys. Lett. B* **788**, 530-534 (2019) doi:10.1016/j.physletb.2018.12.003 [arXiv:1807.05122 [hep-ph]].
- [23] D. Borah, M. Dutta, S. Mahapatra and N. Sahu, *Phys. Rev. D* **105**, no.1, 015004 (2022) doi:10.1103/PhysRevD.105.015004 [arXiv:2110.00021 [hep-ph]].
- [24] L. Coito, C. Faubel, J. Herrero-García, A. Santamaria and A. Titov, *JHEP* **08**, 085 (2022) doi:10.1007/JHEP08(2022)085 [arXiv:2203.01946 [hep-ph]].
- [25] M. Becker, *Eur. Phys. J. C* **79**, no.7, 611 (2019) doi:10.1140/epjc/s10052-019-7095-7 [arXiv:1806.08579 [hep-ph]].
- [26] L. Bian and Y. L. Tang, *JHEP* **12**, 006 (2018) doi:10.1007/JHEP12(2018)006 [arXiv:1810.03172 [hep-ph]].
- [27] C. Cosme, M. Dutra, T. Ma, Y. Wu and L. Yang, *JHEP* **03**, 026 (2021) doi:10.1007/JHEP03(2021)026 [arXiv:2003.01723 [hep-ph]].
- [28] Y. Du, F. Huang, H. L. Li and J. H. Yu, *JHEP* **12**, 207 (2020) doi:10.1007/JHEP12(2020)207 [arXiv:2005.01717 [hep-ph]].
- [29] M. Chianese, B. Fu and S. F. King, *JCAP* **01**, 034 (2021) doi:10.1088/1475-7516/2021/01/034 [arXiv:2009.01847 [hep-ph]].
- [30] A. Liu, F. L. Shao, Z. L. Han, Y. Jin and H. Li, *Eur. Phys. J. C* **83**, no.5, 423 (2023) doi:10.1140/epjc/s10052-023-11609-5 [arXiv:2205.11846 [hep-ph]].
- [31] B. Barman, P. S. Bhupal Dev and A. Ghoshal, *Phys. Rev. D* **108**, no.3, 035037 (2023) doi:10.1103/PhysRevD.108.035037 [arXiv:2210.07739 [hep-ph]].
- [32] A. Liu, F. L. Shao, Z. L. Han, Y. Jin and H. Li, *Phys. Rev. D* **109**, no.5, 055027 (2024) doi:10.1103/PhysRevD.109.055027 [arXiv:2308.12588 [hep-ph]].
- [33] A. Aboubrahim, W. Z. Feng, P. Nath and Z. Y. Wang, *Phys. Rev. D* **103**, no.7, 075014 (2021) doi:10.1103/PhysRevD.103.075014 [arXiv:2008.00529 [hep-ph]].

- [34] A. Aboubrahim, W. Z. Feng, P. Nath and Z. Y. Wang, *JHEP* **06**, 086 (2021) doi:10.1007/JHEP06(2021)086 [arXiv:2103.15769 [hep-ph]].
- [35] W. Z. Feng, Z. H. Zhang and K. Y. Zhang, *JCAP* **05**, 112 (2024) doi:10.1088/1475-7516/2024/05/112 [arXiv:2312.03837 [hep-ph]].
- [36] W. Z. Feng, J. Li and P. Nath, *Phys. Rev. D* **110**, no.1, 015020 (2024) doi:10.1103/PhysRevD.110.015020 [arXiv:2403.09558 [hep-ph]].
- [37] W. Z. Feng and Z. H. Zhang, *Phys. Rev. D* **112**, no.3, 035004 (2025) doi:10.1103/vshn-gbdp [arXiv:2405.19431 [hep-ph]].
- [38] W. Z. Feng, Y. N. Wang and Y. Zhang, to appear.
- [39] L. E. Ibanez and A. M. Uranga, *JHEP* **03**, 052 (2007) doi:10.1088/1126-6708/2007/03/052 [arXiv:hep-th/0609213 [hep-th]].
- [40] M. Cvetič, R. Richter and T. Weigand, *Phys. Rev. D* **76**, 086002 (2007) doi:10.1103/PhysRevD.76.086002 [arXiv:hep-th/0703028 [hep-th]].
- [41] S. Antusch, L. E. Ibanez and T. Macri, *JHEP* **09**, 087 (2007) doi:10.1088/1126-6708/2007/09/087 [arXiv:0706.2132 [hep-ph]].
- [42] M. Cvetič and P. Langacker, *Phys. Rev. D* **78**, 066012 (2008) doi:10.1103/PhysRevD.78.066012 [arXiv:0803.2876 [hep-th]].
- [43] L. E. Ibanez and R. Richter, *JHEP* **03**, 090 (2009) doi:10.1088/1126-6708/2009/03/090 [arXiv:0811.1583 [hep-th]].
- [44] M. Cvetič, J. Halverson, P. Langacker and R. Richter, *JHEP* **10**, 094 (2010) doi:10.1007/JHEP10(2010)094 [arXiv:1001.3148 [hep-th]].
- [45] W. l. Guo and Z. z. Xing, *Phys. Lett. B* **583**, 163-172 (2004) doi:10.1016/j.physletb.2003.12.043 [arXiv:hep-ph/0310326 [hep-ph]].
- [46] J. w. Mei and Z. z. Xing, *Phys. Rev. D* **69**, 073003 (2004) doi:10.1103/PhysRevD.69.073003 [arXiv:hep-ph/0312167 [hep-ph]].
- [47] W. l. Guo, Z. z. Xing and S. Zhou, *Int. J. Mod. Phys. E* **16**, 1-50 (2007) doi:10.1142/S0218301307004898 [arXiv:hep-ph/0612033 [hep-ph]].
- [48] N. Nath, Z. z. Xing and J. Zhang, *Eur. Phys. J. C* **78**, no.4, 289 (2018) doi:10.1140/epjc/s10052-018-5751-y [arXiv:1801.09931 [hep-ph]].
- [49] M. Chianese and S. F. King, *JCAP* **09**, 027 (2018) doi:10.1088/1475-7516/2018/09/027 [arXiv:1806.10606 [hep-ph]].
- [50] M. Chianese, B. Fu and S. F. King, *JCAP* **03**, 030 (2020) doi:10.1088/1475-7516/2020/03/030 [arXiv:1910.12916 [hep-ph]].

- [51] Z. z. Xing and Z. h. Zhao, Rept. Prog. Phys. **84**, no.6, 066201 (2021) doi:10.1088/1361-6633/abf086 [arXiv:2008.12090 [hep-ph]].
- [52] G. Ingelman and J. Rathsman, Z. Phys. C **60**, 243-254 (1993) doi:10.1007/BF01474620
- [53] J. Kersten and A. Y. Smirnov, Phys. Rev. D **76**, 073005 (2007) doi:10.1103/PhysRevD.76.073005 [arXiv:0705.3221 [hep-ph]].
- [54] J. Barry, W. Rodejohann and H. Zhang, JHEP **07**, 091 (2011) doi:10.1007/JHEP07(2011)091 [arXiv:1105.3911 [hep-ph]].
- [55] H. Zhang, Phys. Lett. B **714**, 262-266 (2012) doi:10.1016/j.physletb.2012.06.074 [arXiv:1110.6838 [hep-ph]].
- [56] K. Y. Jung and K. Siyeon, J. Korean Phys. Soc. **81**, no.12, 1211-1224 (2022) doi:10.1007/s40042-022-00674-w [arXiv:2205.13860 [hep-ph]].
- [57] M. Rauch, [arXiv:1610.08420 [hep-ph]].
- [58] P. Achard *et al.* [L3], Phys. Lett. B **517**, 67-74 (2001) doi:10.1016/S0370-2693(01)00993-5 [arXiv:hep-ex/0107014 [hep-ex]].
- [59] J. de Blas, EPJ Web Conf. **60**, 19008 (2013) doi:10.1051/epjconf/20136019008 [arXiv:1307.6173 [hep-ph]].
- [60] K. Cheung, Y. L. Chung, H. Ishida and C. T. Lu, Phys. Rev. D **102**, no.7, 075038 (2020) doi:10.1103/PhysRevD.102.075038 [arXiv:2004.11537 [hep-ph]].
- [61] A. Das, S. Jana, S. Mandal and S. Nandi, Phys. Rev. D **99**, no.5, 055030 (2019) doi:10.1103/PhysRevD.99.055030 [arXiv:1811.04291 [hep-ph]].
- [62] H. Yang, B. Long and C. F. Qiao, Nucl. Phys. B **1004**, 116576 (2024) doi:10.1016/j.nuclphysb.2024.116576 [arXiv:2309.16233 [hep-ph]].
- [63] A. Das, J. Li, S. Mandal, T. Nomura and R. Zhang, Phys. Rev. D **112**, no.3, 035008 (2025) doi:10.1103/df3g-32t9 [arXiv:2410.21956 [hep-ph]].
- [64] M. Blennow, P. Coloma, E. Fernandez-Martinez, J. Hernandez-Garcia and J. Lopez-Pavon, JHEP **04**, 153 (2017) doi:10.1007/JHEP04(2017)153 [arXiv:1609.08637 [hep-ph]].
- [65] P. Astier *et al.* [NOMAD], Phys. Lett. B **570**, 19-31 (2003) doi:10.1016/j.physletb.2003.07.029 [arXiv:hep-ex/0306037 [hep-ex]].
- [66] S. Avvakumov *et al.* [NuTeV], Phys. Rev. Lett. **89**, 011804 (2002) doi:10.1103/PhysRevLett.89.011804 [arXiv:hep-ex/0203018 [hep-ex]].
- [67] D. V. Forero, C. Giunti, C. A. Ternes and M. Tortola, Phys. Rev. D **104**, no.7, 075030 (2021) doi:10.1103/PhysRevD.104.075030 [arXiv:2103.01998 [hep-ph]].
- [68] K. Abe *et al.* [T2K], Phys. Rev. D **103**, no.11, 112008 (2021) doi:10.1103/PhysRevD.103.112008 [arXiv:2101.03779 [hep-ex]].

- [69] M. A. Acero *et al.* [NOvA], Phys. Rev. D **98**, 032012 (2018) doi:10.1103/PhysRevD.98.032012 [arXiv:1806.00096 [hep-ex]].
- [70] P. Adamson *et al.* [MINOS+], Phys. Rev. Lett. **122**, no.9, 091803 (2019) doi:10.1103/PhysRevLett.122.091803 [arXiv:1710.06488 [hep-ex]].
- [71] E. W. Kolb and S. Wolfram, Nucl. Phys. B **172**, 224 (1980) [erratum: Nucl. Phys. B **195**, 542 (1982)] doi:10.1016/0550-3213(82)90012-8
- [72] G. F. Giudice, A. Notari, M. Raidal, A. Riotto and A. Strumia, Nucl. Phys. B **685**, 89-149 (2004) doi:10.1016/j.nuclphysb.2004.02.019 [arXiv:hep-ph/0310123 [hep-ph]].